



Metabolic control analysis of biogeochemical systems



Stilianos Louca ^{1,2}

Many reactive systems involve processes operating at different scales, such as hydrodynamic transport and diffusion, abiotic chemical reactions, microbial metabolism, and population dynamics. Determining the influence of these processes on system dynamics is critical for model design and for prioritizing parameter estimation efforts. Metabolic control analysis is a framework for quantifying the role of enzymes in cellular biochemical networks, but its applicability to biogeochemical and other reactive systems remains unexplored. Here I show how the core concepts of metabolic control analysis can be generalized to much more complex reactive systems, enabling insight into the roles of physical transport, population dynamics, and chemical kinetics at organismal to planetary scales. I demonstrate the power of this framework for two systems of importance to ocean biogeochemistry: A simplified (mostly didactic) model for the sulfate methane transition zone in Black Sea sediments, and a more comprehensive model for the oxygen minimum zone in Saanich Inlet near steady state. I find that physical transport is by far the greatest rate-limiting factor for sulfate-driven methane oxidation in the first system and for fixed nitrogen loss in the second system.

Many reactive systems comprise several processes operating at different spatial and temporal scales, such as cellular metabolism and regulation, enzyme kinetics, microbial population dynamics, abiotic chemical transformations, hydrodynamic and diffusive transport, downward migration of matter in water and sediment columns, tectonic uplift and erosion. Examples of such systems include local or global nitrogen cycling¹, the ocean carbon pump², microbial mats³, material and energy fluxes in food webs⁴, bioreactors, and wastewater treatment plants⁵. Understanding the sensitivity of a system's emergent properties to each of its constituent processes, and identifying the subset of processes that are truly relevant for predictions, is important for multiple reasons. First, parameterizing each of the aforementioned processes in models requires considerable effort; for example, determining microbial metabolic and growth kinetics typically involves laborious incubation experiments^{6,7}. In some microbial systems, physical mixing across space can be the main rate-limiting process, effectively eliminating the dependency on microbial kinetic and population-dynamic parameters^{8,9}. Second, models that account for processes operating at vastly different spatial or temporal scales tend to be computationally expensive^{10–12}, and thus shortcutting some secondary processes could allow for considerable optimization. Third, efficiently steering a system in a specific desired direction, for example, to boost marine productivity or increase wastewater treatment rates, necessitates a determination of the critical “turning knobs”¹³. Flexible and practical mathematical frameworks for performing such analyses are thus highly desirable.

For simple cellular biochemical reaction networks at steady state or quasi-steady-state, metabolic control analysis (MCA) has become a standard mathematical framework for examining the controls that individual enzyme activities exert on fluxes and substrate concentrations^{14–16}. Partial derivatives of the network's responses, including substrate concentrations and fluxes, with respect to enzyme activities are used to define local sensitivity coefficients called concentration control coefficients (CCCs) and flux control coefficients (FCCs), respectively. Due to the particular structure of reaction networks, MCA yields mathematical theorems facilitating the interpretation of FCCs and CCCs, and provides practical guidelines for experimentally determining these coefficients. A notable conceptual impact of MCA has been the realization that many biochemical reaction networks are not governed by a single rate-limiting step, and that their control is instead distributed over multiple steps¹⁷. MCA has been instrumental in studies of cell metabolism, metabolic engineering, and drug development, to name a few applications^{18,19}. To date, MCA has not been generalized to reactive systems with explicit spatial structure or involving processes other than chemical reactions, such as reaction-advection-diffusion models for carbon cycling in sediment columns, microbial communities distributed across a water column, global ocean circulation-biogeochemical models and bioreactors with engineered control loops. Such a generalization would yield novel insights of similar impact as those achieved by MCA in biochemistry. For example, a generalized MCA would facilitate the examination of controls exerted by processes other than enzymatic reactions, such as molecular

¹Department of Biology, University of Oregon, Eugene, OR, USA. ²Institute of Ecology and Evolution, University of Oregon, Eugene, OR, USA.

e-mail: louca.research@gmail.com

diffusion across space, microbial growth, and death, hydrodynamic mixing and sedimentation in the ocean, tectonic uplift in Earth-system models, or hydraulic renewal in wastewater treatment plants.

Here I show how MCA can be elegantly generalized to a much wider class of reactive systems than traditionally considered, including all of the examples mentioned above. In particular, I identify a simple set of conditions, which are widely encountered in reactive systems and which are sufficient for the applicability of MCA. In a nutshell, the most crucial conditions are the existence of a subset of *focal* parameters, whose uniform rescaling leaves the system's steady state unchanged but rescales fluxes by the same factor. As I will show, these parameters are analogous to enzyme activities in biochemical networks analyzed through classical MCA, and a rescaling of these parameters can often be interpreted as a simple rescaling of time. I further define the FCCs and CCCs in a more general form than commonly done for biochemical networks, prove the validity of two important theorems known as the flux and concentration control summation theorems, and provide various examples of models amenable to MCA. I then demonstrate this generalized MCA in detail for two marine systems, each described by a reaction-advection-diffusion partial differential equation model: The sulfate methane transition zone in Black Sea sediments^{20,21}, where I examine the controls of various processes on anaerobic methane oxidation rates, and a seasonal oxygen minimum zone at quasi-steady state in Saanich Inlet²²⁻²⁴, where I examine the controls on microbially driven fixed nitrogen loss.

Results and discussion

Generalizing MCA

I henceforth provide a formal specification of the systems to which MCA shall be generalized, definitions of FCCs and CCCs for such systems, and simple proofs of the famous flux and concentration control summation theorems. As a recurring illustrative example, I will consider a general reaction-advection-diffusion partial differential equation (PDE) model on a finite 1-dimensional interval:

$$\frac{\partial U_j}{\partial t} = \frac{\partial}{\partial z} \left[D_j(z) \frac{\partial U_j}{\partial z} \right] - \frac{\partial}{\partial z} \left(v_j(z) \cdot U_j(z) \right) + S_j(z, \mathbf{U}), \quad (1)$$

where z represents the single spatial coordinate within the interval $\mathcal{Z} = [a, b]$, the dynamic variables U_1, \dots, U_m are scalar fields on \mathcal{Z} defining the system's state at any moment in time, D_1, \dots, D_m are given location-dependent diffusivities, v_1, \dots, v_m are given location-dependent advection speeds and S_1, \dots, S_m are source terms (e.g., accounting for chemical or biological processes). For example, z may represent depth along a water or sediment column, and each U_j may represent the concentration of a specific substance or the population density of a microbial species. While the above model is a priori dynamical, I will henceforth focus on its steady states, i.e., the case where $\partial U_j / \partial t = 0$. For illustration, at the first boundary I consider fixed-value conditions:

$$U_j(a) = A_j, \quad (2)$$

whereas at the second boundary I consider fixed-flux conditions:

$$v_j(b)U_j(b) - D_j(b) \frac{\partial U_j}{\partial z} \Big|_{z=b} = B_j, \quad (3)$$

where A_1, \dots, A_m and B_1, \dots, B_m are constants. Other types of boundary conditions, including more general Robin boundary conditions²⁵, are also possible. Additional examples are given throughout the article and in Supplementary Discussion 1. In particular, Supplementary Discussion 1.1 elaborates on how the general concepts presented here relate to classical MCA, while Supplementary Discussion 1.3 exemplifies these concepts on a 3-dimensional carbon cycle PDE model overlaid on an ocean general circulation model.

State space: I consider dynamical systems at (quasi-)steady state, whose state at any point in time is described by a vector-valued function \mathbf{U} defined

on some arbitrary domain \mathcal{Z} , i.e., $\mathbf{U} : \mathcal{Z} \rightarrow \mathbb{R}^m$. Let \mathcal{U} denote the set of all possible system states. Here, m represents the number of dynamic physical/biological variables, such as chemical concentrations or biological species densities. For a well-mixed system described by an ordinary differential equation model, such as biochemical reaction networks considered in classical MCA¹⁵, \mathcal{Z} is a single point and thus \mathbf{U} is just a vector of m numbers, whereas for an ordinary differential equation box-model with multiple connected boxes, \mathcal{Z} is an enumeration of the boxes and thus \mathbf{U} comprises m numbers for each of the boxes. In the case of a diffusion-advection PDE model in 3 spatial dimensions, \mathcal{Z} represents the 3 spatial axes (i.e., \mathcal{Z} is a subset of \mathbb{R}^3), \mathbf{U} represents m scalar fields defined at each point in space, and \mathcal{U} represents the space of acceptable fields (for example, the set of twice-continuously differentiable functions $\mathcal{Z} \rightarrow \mathbb{R}^{m \times 26}$). For the PDE example given in Eq. (1), \mathcal{Z} is simply the interval $[a, b]$ and each \mathbf{U} represents m curves on $[a, b]$.

Henceforth, let $\mathbf{p} \in \mathbb{R}^n$ denote n focal model parameters of interest. Note that \mathbf{p} does not need to comprise all conceivable model parameters, but rather represents a focal subset of n parameters with respect to which we will be examining the system's sensitivity. All other model parameters not included in \mathbf{p} are assumed fixed throughout. In the PDE model in Eq. (1), \mathbf{p} could for example include the assumed advection velocities, the imposed boundary fluxes B_j , and so on. Later, I will discuss specific conditions that \mathbf{p} must satisfy in order for MCA to be applicable.

Definition of steady state: Assume that for any given value of \mathbf{p} , the steady state is uniquely defined as the solution to the following set of abstract equations:

$$F_\omega(\mathbf{U}, \mathbf{p}) = 0, \quad (4)$$

where the index ω takes values in some arbitrary set Ω , and each F_ω is a scalar-valued function that imposes a condition on \mathbf{U} , i.e., $F_\omega : \mathcal{U} \times \mathbb{R}^n \rightarrow \mathbb{R}$. The form of each F_ω can be quite broad, including algebraic, differential and even integral equations. Similarly, Ω may in principle be arbitrary, although in practice it will be closely related to the domain \mathcal{Z} and the number of variables m . For example, in the case of a single-box ordinary differential equation model, Ω would be $\{1, \dots, m\}$ and F_1, \dots, F_m would constitute m algebraic equations that fully determine the steady state. In the case of a PDE model on a finite 3-dimensional domain, Ω would be $\mathcal{Z} \times \{1, \dots, m\}$, with F_ω encoding the PDE in the interior of \mathcal{Z} as well as the boundary conditions at the boundary of \mathcal{Z} . For the PDE example in Eq. (1), Ω is $[a, b] \times \{1, \dots, m\}$, with steady-state conditions being:

$$\begin{aligned} z \in (a, b) : F_{z,j}(\mathbf{U}) &= \frac{\partial}{\partial z} \left[D_j(z) \frac{\partial U_j}{\partial z} \right] - \frac{\partial}{\partial z} \left(v_j(z) \cdot U_j(z) \right) + S_j(z, \mathbf{U}), \\ z = a : F_{a,j}(\mathbf{U}) &= U_j(a) - A_j, \\ z = b : F_{b,j}(\mathbf{U}) &= v_j(b)U_j(b) - D_j(b) \frac{\partial U_j}{\partial z} \Big|_{z=b} - B_j, \end{aligned} \quad (5)$$

where for simplicity I omitted writing out the focal parameters \mathbf{p} in the various terms above. For any given value of \mathbf{p} , let $\bar{\mathbf{U}}(\mathbf{p}) \in \mathcal{U}$ be the corresponding steady state, i.e. satisfying

$$F_\omega(\bar{\mathbf{U}}(\mathbf{p}), \mathbf{p}) = 0 \quad (6)$$

for all $\omega \in \Omega$.

Scaling invariance of steady state: We are now ready to specify the first major condition for MCA. Assume that uniformly rescaling the parameters \mathbf{p} by an arbitrary positive constant $\alpha > 0$ does not change the steady state, in other words:

$$\bar{\mathbf{U}}(\alpha \mathbf{p}) = \bar{\mathbf{U}}(\mathbf{p}). \quad (7)$$

The above invariance condition is the most critical condition that a system and the focal parameters must satisfy, in order for MCA to be applicable.

Importantly, whether Eq. (7) is satisfied or not depends on which parameters are included in \mathbf{p} . As an example, in biochemical reaction networks considered by classical MCA¹⁵, \mathbf{p} typically represents the activities of enzymes, while other parameters such as stoichiometric coefficients are kept fixed. In these models, reaction rates are assumed to scale linearly with enzyme activities when substrate concentrations are kept constant, and steady-state concentrations of metabolites remain unchanged if all enzyme activities are modified by the same factor while keeping all other parameters fixed (details in Supplementary Discussion 1.1). As illustrated in further examples below, basic familiarity with the system and mathematical intuition are often sufficient for recognizing a proper subset of focal parameters, however, in some cases the task may be more complicated. Below, all control coefficients will be defined with respect to these focal parameters \mathbf{p} . It is worth mentioning that condition (7) is equivalent to the condition that each F_ω satisfies:

$$F_\omega(\bar{\mathbf{U}}(\mathbf{p}), \alpha\mathbf{p}) = 0, \tag{8}$$

for all $\alpha > 0$. It is clear that if F_ω is positively homogeneous in \mathbf{p} , that is, satisfies:

$$F_\omega(\mathbf{U}, \alpha\mathbf{p}) = \alpha^\kappa F_\omega(\mathbf{U}, \mathbf{p}) \tag{9}$$

for some fixed $\kappa \in \mathbb{R}$ and for all \mathbf{p} , all $\mathbf{U} \in \mathcal{U}$ and all $\alpha > 0$, then F_ω would necessarily also satisfy condition (8). Note that the exponent κ may in principle depend on ω . I stress that homogeneity of F_ω in \mathbf{p} is a *stronger* condition than condition (8) or the equivalent (7), in other words condition (9) always implies (8) and (7), but not the other way around. Nevertheless, as the examples below will show, homogeneity is often satisfied and easy to recognize.

Concentration control coefficients: We are now ready to define the first set of control coefficients, known in classical MCA as *concentration control coefficients* (CCCs). Consider a scalar quantity of interest C that can be expressed as a function solely of \mathbf{U} and not explicitly depending on \mathbf{p} , that is, C is fully determined by \mathbf{U} and thus $C : \mathcal{U} \rightarrow \mathbb{R}$. For any given \mathbf{p} , define $\bar{C}(\mathbf{p})$ as the corresponding steady state value of C , i.e., $\bar{C}(\mathbf{p}) := C(\bar{\mathbf{U}}(\mathbf{p}))$. For example, in a biochemical reaction network C may be the concentration of a specific metabolite. In the PDE example in Eq. (1), C may be U_j at a specific location z , i.e., $C(\mathbf{U}) = U_j(z)$, or it may be the average value of U_j , i.e., $C(\mathbf{U}) = \frac{1}{b-a} \int_a^b U_j(z) dz$. To emphasize the analogy to classical MCA, I henceforth refer to C as a *concentration* regardless of its precise nature. The CCCs of this concentration are defined as:

$$\mu_i := \frac{p_i}{\bar{C}} \cdot \frac{\partial \bar{C}}{\partial p_i}, \tag{10}$$

where $i \in \{1, \dots, n\}$ enumerates all focal parameters. In classical MCA, one typically considers the concentrations of all metabolites, and thus one obtains a distinct CCC for each metabolite and for each enzyme. Each μ_i is a unitless number that quantifies the relative change in \bar{C} under an infinitesimal change in the parameter p_i . In the context of generic sensitivity analysis, such coefficients are also known as *normalized local sensitivity coefficients*²⁷. Each CCC only encodes a local sensitivity, i.e., the response to small changes, and may (and usually does) depend on \mathbf{p} . Recall that we assumed that $\bar{\mathbf{U}}$ is invariant under a uniform rescaling of \mathbf{p} , which means that \bar{C} is also invariant. By Euler’s homogeneous function theorem²⁸, it follows that:

$$0 = \sum_{i=1}^n p_i \cdot \frac{\partial \bar{C}}{\partial p_i}. \tag{11}$$

Dividing Eq. (11) by \bar{C} yields the famous concentration control summation theorem:

$$\sum_{i=1}^n \mu_i = 0. \tag{12}$$

The theorem essentially asserts that the controls of the various focal parameters on any given “concentration” cancel each other out, with some parameters having negative controls and others having positive controls.

Flux control coefficients: We now consider the control that the focal parameters \mathbf{p} exert on fluxes. As will become more clear in the definition below and in later examples, the meaning of *flux* is kept quite broad in this article, and may include the rate of a reaction in a biochemical network, or the net consumption rate of a substrate by multiple reactions, or the vertical flux of a substance across a sediment column, or the cell production rate for a specific microbial species. Specifically, suppose that our flux of interest can be expressed as a function $J : \mathcal{U} \times \mathbb{R}^n \rightarrow \mathbb{R}$ that depends on \mathbf{U} and \mathbf{p} and that is positively 1-homogeneous in \mathbf{p} , that is, it satisfies:

$$J(\mathbf{U}, \alpha\mathbf{p}) = \alpha J(\mathbf{U}, \mathbf{p}) \tag{13}$$

for all $\alpha > 0$. The above condition is the second-most critical condition that a system must satisfy for MCA of fluxes in this article (the first one being Eq. (7)). Intuitively, the above homogeneity condition states that uniformly rescaling all focal parameters \mathbf{p} by a positive factor, while keeping the system state fixed, should modulate the flux by that same factor. For example, in classical MCA, uniformly altering all enzyme activities by the same factor, while keeping metabolite concentrations fixed, increases each reaction rate by that same factor. In the PDE model in Eq. (1), increasing all diffusion coefficients and advection speeds uniformly by the same factor while keeping \mathbf{U} unchanged, would increase flux rates across space by that same factor. In some atypical cases, substantial system expertise may be needed to find a good set of focal parameters \mathbf{p} in conjunction with proper flux functions so as to satisfy Eq. (13), in addition to satisfying the scaling invariance condition (7) for $\bar{\mathbf{U}}$. For any given \mathbf{p} , let $\bar{J}(\mathbf{p})$ be the flux at steady state:

$$\bar{J}(\mathbf{p}) := J(\bar{\mathbf{U}}(\mathbf{p}), \mathbf{p}). \tag{14}$$

We are now ready to define a second set of control coefficients, known in classical MCA as *flux control coefficients* (FCCs):

$$\nu_i := \frac{p_i}{\bar{J}} \cdot \frac{\partial \bar{J}}{\partial p_i}, \tag{15}$$

where $i \in \{1, \dots, n\}$ enumerates all focal parameters. Each ν_i is a unitless number that quantifies the relative change in the steady state flux $\bar{J}(\mathbf{p})$ under an infinitesimal change in the parameter p_i . Note that FCCs are specific to the flux considered, i.e., one would obtain a separate set of FCCs if one were to consider a different flux. Similarly to CCCs, a summation theorem can also be derived for FCCs, as follows. For any \mathbf{p} and any $\alpha > 0$ we have:

$$\bar{J}(\alpha\mathbf{p}) \stackrel{(14)}{=} J(\bar{\mathbf{U}}(\alpha\mathbf{p}), \alpha\mathbf{p}) \stackrel{(7)}{=} J(\bar{\mathbf{U}}(\mathbf{p}), \alpha\mathbf{p}) \stackrel{(13)}{=} \alpha J(\bar{\mathbf{U}}(\mathbf{p}), \mathbf{p}) \stackrel{(14)}{=} \alpha \bar{J}(\mathbf{p}), \tag{16}$$

in other words, \bar{J} is positively 1-homogeneous. By Euler’s homogeneous function theorem²⁸ it thus follows that:

$$\bar{J}(\mathbf{p}) = \sum_{i=1}^n p_i \cdot \frac{\partial \bar{J}(\mathbf{p})}{\partial p_i}. \tag{17}$$

Dividing both sides of Eq. (17) by \bar{J} yields the famous flux control summation theorem:

$$\sum_{i=1}^n \nu_i = 1. \tag{18}$$

The theorem asserts that the FCCs of a given flux must sum to 1. In many cases (but not always, e.g.²⁹), the FCCs are non-negative numbers, and can thus be interpreted as fractional contributions to the overall control of a flux. For example, in classical MCA the FCCs for any given reaction rate correspond to the controls exerted by the reaction network’s individual

enzymes, which in many cases (e.g., for linear pathways) are all non-negative. In such cases no more than one of the parameters may exert full control with an FCC near 1. At least in classical MCA, typically all FCCs are much lower than 1, i.e., none of the enzymes is of major importance in and of itself, and major changes in flux are only achievable by simultaneously changing multiple enzyme activities^{17,29}. Whether this situation also turns out to be common in other systems, accessible to the generalized MCA described here, is an open question (e.g., see simulation examples below).

Intuitive interpretation of focal parameters: It should be clear now that the applicability of MCA, including the CCC and FCC summation theorems, requires the recognition of a proper set of parameters, here referred to as focal. In principle, there may exist multiple alternative sets of focal parameters in a model, and this is more likely to occur in more redundantly parameterized models. Typically, one set of focal parameters will stand out as more intuitive, interesting and/or less trivial. In many biogeochemical models, including the two examples discussed in detail below as well as the examples in Supplementary Discussion 1, an intuitive and non-trivial set of focal parameters can be obtained by considering all *rate*-like parameters such as microbial per-capita death rates, reaction rate coefficients, outgassing rate coefficients, advection velocities, diffusivities, sedimentation rates and so on, as well as the inverses of all *time*-like parameters such as half-lifetimes of decay processes. Such parameters can usually (but not always) be readily recognized based on their physical units, for example because they explicitly include time or inverse time (e.g., seconds or per-second) or because they can be redefined in such a manner (e.g., Watt = Joules per second). Generally, such parameters determine the time scales of various processes in the system, and ultimately set the “pace” of the system’s dynamics. Multiplying all such parameters by the same factor α thus corresponds to a simple linear rescaling of time, which in and of itself leaves the steady state unchanged (scaling invariance condition in Eq. (7)) but modulates process rates and fluxes by that factor (homogeneity condition in Eq. (13)). Similar time-scaling arguments have been made before for classical MCA^{30–32}. FCCs with respect to such parameters yield insight into the rate-limiting effects that individual processes potentially operating at different time scales (e.g. chemical reactions, physical transport, biological growth) have on energy and material fluxes in a system. Note that while the above serves as a rough intuitive guideline for finding a set of focal parameters, the conditions discussed above (Eqs. (7) and (13)) should always be checked for any candidate set of focal parameters.

Grouping parameters: In some cases, the number of parameters that must be included in \mathbf{p} in order to achieve scaling invariance of the steady state (Eq. (7)) and homogeneity of fluxes (Eq. (13)) can be quite large, and the control coefficients associated with each such parameter will tend to be close to zero. For example, in reaction-advection-diffusion models such as the PDE in Eq. (1) diffusivity may vary across space, in which case diffusivity alone comprises multiple parameters — in the extreme case, a separate diffusivity per grid point^{33,34}. In such cases it can be helpful to combine multiple similar parameters into a single group to evaluate their overall control on the system. In the following I explain how such a grouping might be achieved, and how the control coefficients of a parameter group relate to the control coefficients of the original grouped parameters.

Let \mathbf{p} be a set of focal parameters satisfying the MCA assumptions discussed above (Eqs. (7) and (13)), and suppose that we wish to combine the first k parameters, i.e., p_1, \dots, p_k , into a single new parameter \tilde{p}_1 . This representative parameter may be set, for example, to the average of the original p_1, \dots, p_k , although many other representations are conceivable. We henceforth define $q_i := p_i/\tilde{p}_1$ for $i = 1, \dots, k$, so that we can express the original parameters as $p_i = \tilde{p}_1 \cdot q_i$. We thus obtain a reduced set of $n - k + 1$ focal parameters, $\tilde{p}_1, \tilde{p}_2 := p_{k+1}, \dots, \tilde{p}_{n-k+1} := p_n$, collectively denoted as a vector $\tilde{\mathbf{p}}$. Importantly, while the q_1, \dots, q_k remain essential for the full model specification, they are henceforth kept fixed and are no longer considered for MCA. Thus, we can ask what happens to the steady state when \tilde{p}_1 is varied while the q_1, \dots, q_k remain fixed. The new focal parameters $\tilde{\mathbf{p}}$ again satisfy the MCA assumptions (Eqs. (7) and (13)). Indeed, uniformly rescaling $\tilde{\mathbf{p}}$ by a factor α is equivalent to rescaling the original \mathbf{p} by that factor,

which by assumption keeps $\bar{\mathbf{U}}$ unchanged and changes J by the factor α . The CCC of any concentration with respect to \tilde{p}_1 is:

$$\tilde{\mu}_1 := \frac{\tilde{p}_1}{\bar{C}} \cdot \frac{\partial \bar{C}}{\partial \tilde{p}_1} = \frac{\tilde{p}_1}{\bar{C}} \cdot \sum_{i=1}^k \frac{\partial \bar{C}}{\partial p_i} \cdot \frac{\partial p_i}{\partial \tilde{p}_1} \stackrel{(10)}{=} \frac{\tilde{p}_1}{\bar{C}} \cdot \sum_{i=1}^k \frac{\bar{C}}{p_i} \cdot \mu_i q_i = \sum_{i=1}^k \mu_i \quad (19)$$

Thus, a CCC with respect to \tilde{p}_1 is simply the sum of CCCs with respect to the original represented parameters p_1, \dots, p_k . Similarly, the FCC with respect to \tilde{p}_1 is:

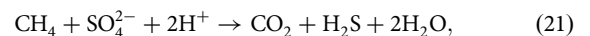
$$\tilde{\nu}_1 := \frac{\tilde{p}_1}{\bar{J}} \cdot \frac{\partial \bar{J}}{\partial \tilde{p}_1} = \frac{\tilde{p}_1}{\bar{J}} \cdot \sum_{i=1}^k \frac{\partial \bar{J}}{\partial p_i} \cdot \frac{\partial p_i}{\partial \tilde{p}_1} \stackrel{(15)}{=} \frac{\tilde{p}_1}{\bar{J}} \cdot \sum_{i=1}^k \frac{\bar{J}}{p_i} \cdot \nu_i q_i = \sum_{i=1}^k \nu_i \quad (20)$$

Thus, an FCC with respect to \tilde{p}_1 is the sum of FCCs with respect to the original represented parameters. Intuitively speaking, the control exerted by \tilde{p}_1 on a steady state concentration or a steady state flux is the sum of controls that would be exerted individually by the p_1, \dots, p_k .

Example: Sulfate-methane transition zone in Black Sea sediments

As a first detailed example, I examine a simple PDE model for a sulfate-methane transition zone (SMTZ) in Black Sea sediments^{20,21}. SMTZs are widespread zones in marine sediments where methane diffusing upward from deep sediments is oxidized by microbial consortia using downward moving sulfate as a terminal electron acceptor³⁵. The sulfate itself is reduced to hydrogen sulfide, a toxin to many organisms, which accumulates locally but is ultimately consumed by processes on both ends of the SMTZ. SMTZs effectively act as a barrier to methane that might otherwise be released into the water and ultimately the atmosphere. The efficacy of this barrier in principle depends on the kinetics of local chemical reactions involved in the sulfur and methane cycles, as well as rates of diffusive/advection transport across the sediment column. The goal of this section is to examine the controls that these factors exert on methane oxidation rates and sulfide accumulation.

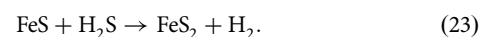
The model is based on insights by Jørgensen et al.²⁰ and Egger et al.²¹, and captures the major microbial and physical processes governing methane and sulfur fluxes in the top 600 cm of sediments. Specifically, the model is a system of 1-dimensional reaction-advection-diffusion PDEs across the sediment column, for the concentrations of $m = 6$ dynamic metabolites: Methane (CH_4), sulfate (SO_4^{2-}), hydrogen sulfide (H_2S), divalent iron (Fe^{2+}), iron sulfide (FeS) and pyrite (FeS_2). All metabolites are subject to downward advection due to sedimentation, while dissolved metabolites are additionally transported via molecular diffusion. Molecular diffusivities are adjusted for sediment porosity²¹ and are thus depth-dependent. Metabolites are coupled through 3 chemical reactions: Microbially driven anaerobic oxidation of methane using sulfate (AOM):



formation of iron sulfide (FIS):



and formation of pyrite (FP):



Thus, each metabolite’s concentration U_j ($\text{mol} \cdot \text{L}^{-1}$) satisfies the following PDE:

$$\frac{\partial U_j}{\partial t} = \frac{\partial}{\partial z} \left[D_j(z) \frac{\partial U_j}{\partial z} \right] - \frac{\partial}{\partial z} \left(v_j(z) \cdot U_j(z) \right) + \sum_{r=1}^3 S_{jr} R_r(\mathbf{U}(z)), \quad (24)$$

where z denotes depth, D_j is the depth-dependent diffusivity ($\text{cm}^2 \cdot \text{yr}^{-1}$) and v_j the depth-dependent downward advection speed ($\text{cm} \cdot \text{yr}^{-1}$) for the j th metabolite, \mathbb{S} is the stoichiometric matrix of the reactions and R_r is the rate of the r -th reaction ($\text{mol} \cdot \text{L}^{-1} \cdot \text{yr}^{-1}$). While the diffusivities are different for each metabolite, advection speeds only differ between solids and dissolved metabolites; apart from these factors, diffusivities and advection speeds are largely determined by the sedimentation rate, sediment density and the porosity profile (Supplementary Discussion 2). The above model is a priori dynamical, however, we henceforth focus on its steady states, i.e., where $\partial U_j / \partial t = 0$. Reaction kinetics are expressed as mass action laws, i.e., 1st order in each substrate:

$$R_r(\mathbf{U}) = \beta_r \prod_{j \in L_r} U_j, \quad (25)$$

where β_r is a constant rate coefficient (henceforth “affinity”) and L_r specifies the substrates for the r -th reaction (e.g., CH_4 and SO_4^{2-} for methane oxidation). Note that mass action laws can be seen as approximations of common higher-order rate laws when substrate concentrations are low^{36,37}. This model does not track and does not explicitly account for microbial population dynamics. Boundary conditions on both ends, i.e., at $a = 0$ and $b = 600$ cm, are in the form of fixed values for all metabolites:

$$U_j(a) = A_j, \quad U_j(b) = B_j, \quad (26)$$

where A_j and B_j are constants. For any given choice of parameters, the corresponding steady state $\bar{\mathbf{U}}$ was computed by integrating the PDE forward in time until convergence. For additional details, including model parameterization, boundary values and numerical simulation scheme, see Supplementary Discussion 2 and Supplemental Tables S1 and S2. The steady state for default parameters is shown in Fig. 1A–F, with corresponding net production rates of metabolites shown in Fig. 1G–L. Consistent with general expectations^{20,21}, methane oxidation takes place in a narrow zone at intermediate depth, where methane and sulfate concentrations both converge to zero. Hydrogen sulfide generated by this process either escapes past the sediment–water interface at the top, or is consumed through the formation of pyrite below (Fig. 1E, K). Iron sulfide (Eq. (22)) mostly acts as an intermediate to the eventual formation of pyrite (Eq. (23)).

Steady state conditions and focal parameters: Following the notation introduced in Eq. (5), the system’s steady state conditions are the solutions to the following set of equations:

$$\begin{aligned} a < z < b: \quad 0 &= F_{z,j}(\mathbf{U}, \mathbf{p}) := \frac{\partial}{\partial z} \left[D_j(z) \frac{\partial U_j}{\partial z} \right] - \frac{\partial}{\partial z} \left(v_j(z) U_j(z) \right) + \sum_{r=1}^3 \mathbb{S}_{jr} \beta_r \prod_{j \in L_r} U_j(z), \\ z = a: \quad 0 &= F_{a,j}(\mathbf{U}, \mathbf{p}) := U_j(a) - A_j, \\ z = b: \quad 0 &= F_{b,j}(\mathbf{U}, \mathbf{p}) := U_j(b) - B_j. \end{aligned} \quad (27)$$

So far we have not yet specified which of the model parameters should be focal, which is necessary in order to fully apply MCA. As a reminder, focal parameters must at least satisfy the invariance condition for steady states in Eq. (7) or equivalently Eq. (8). If fluxes are to be analyzed, focal parameters must also satisfy the homogeneity condition for fluxes in Eq. (13). Following the earlier guideline on determining a set of focal parameters, one may consider all rate-like parameters in the model, namely the diffusivities D_j , the advection speed v_j and the affinities β_r . For illustration, these are highlighted below using arrows in the first set of steady-state conditions, copied from Eq. (27):

$$a < z < b \quad F_{z,j}(\mathbf{U}, \mathbf{p}) = \frac{\partial}{\partial z} \left[\underset{\uparrow}{D_j(z)} \frac{\partial U_j}{\partial z} \right] - \frac{\partial}{\partial z} \left(v_j(z) \underset{\uparrow}{U_j(z)} \right) + \sum_{r=1}^3 \mathbb{S}_{jr} \underset{\uparrow}{\beta_r} \prod_{j \in L_r} U_j(z). \quad (28)$$

Note that there are no time-like parameters in this model. Uniformly rescaling the D_j , v_j and β_r with a constant factor (while keeping \mathbf{U} fixed) rescales the right hand side of Eq. (28) by the same factor, thus satisfying the homogeneity condition in Eq. (9) with $\kappa = 1$, for all $F_{z,j}$, where $a < z < b$. Further, rescaling these parameters (again, while keeping \mathbf{U} fixed) has no effect on the boundary conditions, i.e., $F_{a,j}(\mathbf{U}, \mathbf{p}) = F_{a,j}(\mathbf{U}, \mathbf{p})$ and $F_{b,j}(\mathbf{U}, \mathbf{p}) = F_{b,j}(\mathbf{U}, \mathbf{p})$, thus satisfying the homogeneity condition in Eq. (9) with $\kappa = 0$. Thus, collectively the D_j , v_j and β_r indeed constitute a suitable set of focal parameters. Intuitively, these parameters define the “pace” of the system’s dynamics, and uniformly rescaling these parameters corresponds to a simple rescaling of time, which always preserves steady states. Uniformly rescaling all focal parameters by a factor (while keeping \mathbf{U} fixed) also rescales each reaction rate R_r by that same factor, and thus reaction rates satisfy the homogeneity condition for fluxes in Eq. (13). This conclusion remains valid even when considering the mean reaction rates, i.e., averaged over the entire depth range.

I stress that the invariance condition for steady states would no longer hold if one omitted any single one of D_j , v_j or β_r from the set of focal parameters. For example, if one were to only consider the D_j and β_r as focal parameters, then replacing \mathbf{p} by $\alpha \mathbf{p}$ (while keeping \mathbf{U} fixed) would no longer rescale the right-hand side of Eq. (28) by α , since the advection term would remain unchanged while the diffusion and source terms would change by a factor α . Intuitively, this would correspond to a rescaling of time (change in pace) for only a subset of processes (diffusion and reactions), while keeping time unscaled for advection, thus changing the balance between these three processes and ultimately altering the steady state.

The boundary concentrations A_j and B_j cannot be included as focal parameters, since this would violate the invariance condition for steady states. Indeed, changes in A_j or B_j would inevitably change the system’s steady state, at least at the boundary and in its vicinity, regardless of how the other model parameters are varied. For the stoichiometric coefficients \mathbb{S}_{jr} , the situation is more subtle. For example, if one or more stoichiometric coefficients were to be included in \mathbf{p} along with the D_j , v_j , β_r , then replacing \mathbf{p} by $\alpha \mathbf{p}$ while keeping \mathbf{U} fixed would generally not rescale the right-hand side of Eq. (28) by that same factor. However, if one were to omit all affinities β_r and instead include all stoichiometric coefficients in \mathbf{p} , while also keeping the diffusivities D_j and advection speeds v_j , then one would again obtain a set of focal parameters. This is intuitive and may even be considered trivial, since uniformly rescaling all stoichiometric coefficients is equivalent to uniformly rescaling all reaction affinities, but it serves to highlight the fact that a model may in principle exhibit more than one possible set of focal parameters. A similar ambiguity exists in classical MCA, where one could in principle focus on stoichiometric coefficients instead of enzyme concentrations. In practice this is virtually never done, since stoichiometric coefficients are generally considered fixed and/or normalized according to some convention, for example such that electron acceptors have a coefficient of 1, or such that the coefficients of a reaction are co-prime.

Following the earlier discussion on grouping parameters, for simplicity I henceforth group the diffusivities of each metabolite across space. Specifically, I consider the average diffusivities $\bar{D}_j := \frac{1}{b-a} \int_a^b D_j(z) dz$, while keeping the location-dependent normalized diffusivities $\bar{d}_j(z) := D_j(z) / \bar{D}_j$ fixed. Due to the strong relationships between advection speeds, we group all advection speeds across space and across all metabolites into a single average, \bar{v} , while keeping the metabolite- and location-dependent normalized advection speeds $\bar{v}_j(z) := v_j(z) / \bar{v}$ fixed. Thus, the vector of focal parameters considered for MCA is:

$$\mathbf{p} = (\bar{D}_{\text{CH}_4}, \bar{D}_{\text{SO}_4^{2-}}, \bar{D}_{\text{H}_2\text{S}}, \bar{D}_{\text{Fe}^{2+}}, \bar{D}_{\text{FeS}}, \bar{D}_{\text{FeS}_2}, \bar{v}, \beta_{\text{AOM}}, \beta_{\text{FIS}}, \beta_{\text{FP}}). \quad (29)$$

Control coefficients: We are now ready to examine the FCCs of the mean rate of methane oxidation and the CCCs of the mean concentration of hydrogen sulfide with respect to the above focal parameters (Eqs. (15) and (10), respectively). Numerically, the control coefficients can be estimated via centered difference quotients, i.e., by varying one parameter at a time by a small amount and examining the corresponding small changes in the steady

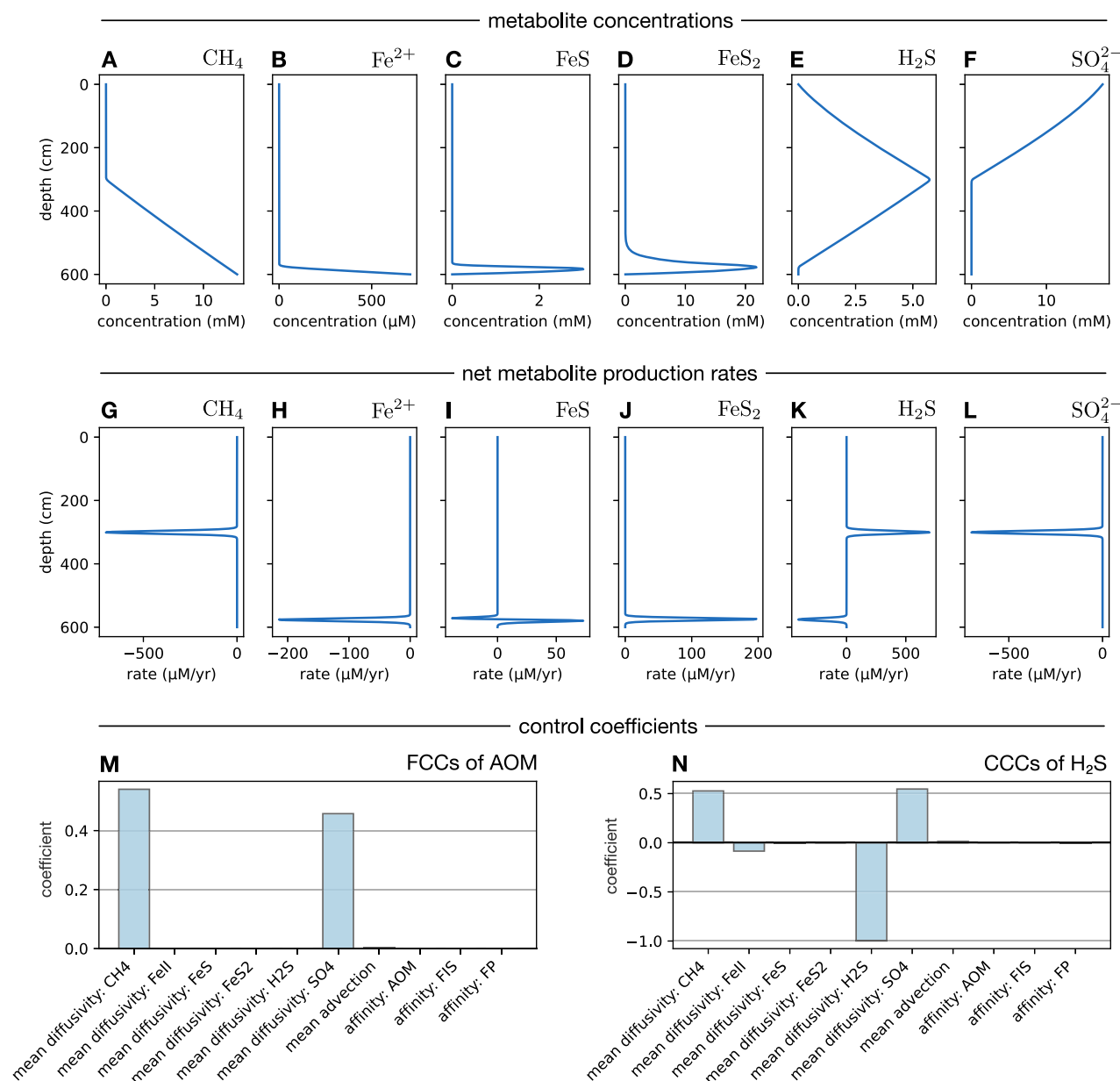


Fig. 1 | Black Sea SMTZ. A–F Steady state metabolite concentrations across the Black Sea sediment column (0–600 cm), as predicted by the PDE model. G–L Predicted steady state net production rates of metabolites. A negative rate indicates a net consumption. The restriction of chemical activity to narrow zones is

typical for transport-limited systems^{8,9}. **M** Flux control coefficients for the rate of anaerobic methane oxidation (AOM). **(N)** Control coefficients for the average concentration of hydrogen sulfide.

state (details in Supplementary Discussion 2). FCCs for the mean methane oxidation rate (Fig. 1M) are all positive, and — due to the FCC summation theorem — can thus be interpreted as fractions of overall control. By far the most important FCCs are those associated with methane diffusivity and sulfate diffusivity, which together contribute about 99.8% of the control, while advection speed contributes about 0.2% of the control. In contrast, the FCC associated with the reaction’s affinity (β_{AOM}) is essentially zero (up to numerical error). Thus, the rate of methane oxidation appears to be nearly entirely controlled by the molecular diffusion rates of methane and sulfate, with downward advection contributing a detectable but minuscule part, and reaction affinity exerting practically no control at all. Ultimately, this dominance of transport as a controlling factor stems from the vast difference in time scales involved in vertical transport across the sediment column and the chemical reactions. Under these conditions, AOM is restricted to a narrow depth zone, whose location and total reaction rate is largely

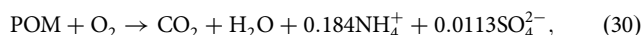
determined by the reaction stoichiometry, the imposed boundary conditions and the diffusivities of methane and sulfide^{8,9}. Hypothetically, if reaction rates were much slower or diffusion much faster, to the point where their time scales become comparable, reactions would not be confined to a narrow zone and their rates would be partly controlled by kinetic parameters. Indeed, repeating the above analysis with 10^5 times lower affinities, substantially widens the zone where each reaction occurs, and makes FCCs associated with affinities comparable to those associated with diffusivities (Fig. S1).

CCCs for mean H₂S concentration (Fig. 1N) are largely dominated by the diffusivities of methane and sulfate (positive control) and the diffusivity of H₂S (negative control), followed by the much weaker (but detectable) controls associated with the diffusivity of Fe²⁺ (negative) and advection speed (positive). CCCs associated with reaction affinities have negligible control on the mean H₂S concentration. Thus, the extent of H₂S

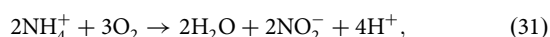
accumulation is largely determined by a balance between methane and sulfate transport (which controls H₂S production rates) and H₂S transport away from the area of production. Note that while some CCCs are positive and some are negative, as predicted by the concentration control summation theorem positive and negative CCCs ultimately cancel each other out.

Example: Fixed nitrogen loss in a seasonal oxygen minimum zone

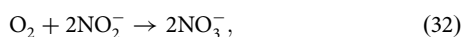
As a second detailed example, I examine a 1-dimensional PDE model for microbial populations and microbially driven redox reactions in a seasonal oxygen minimum zone (OMZ) in Saanich Inlet, off the coast of Vancouver Island^{23,24}. OMZs are regions in the ocean water column where oxygen-poor conditions favor microbial anaerobic metabolisms, which commonly result in the conversion of bioavailable (fixed) nitrogen to dinitrogen (N₂)³⁸. OMZs thus act as sinks for bioavailable nitrogen in the ocean, with major implications for marine ecosystems³⁹. The model considered here was previously described and fitted to data by Louca et al.²², and hence here only an overview is given. The model is constructed to reproduce the quasi-steady state established in the Saanich Inlet water column in early 2010, during a period of intense stratification. The model tracks the concentrations of dissolved ammonium (NH₄⁺), oxygen (O₂), nitrate (NO₃⁻), nitrite (NO₂⁻), hydrogen sulfide (H₂S), nitrous oxide (N₂O), sulfate (SO₄²⁻) and dinitrogen (N₂), between depths $a = 100$ m and $b = 200$ m. The dynamics of these metabolites are coupled through 5 microbially driven reactions: Aerobic remineralization of particulate organic matter (AEROM):



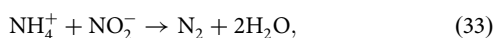
aerobic ammonium oxidation to nitrite (AAO):



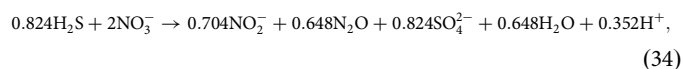
aerobic nitrite oxidation to nitrate (ANO):



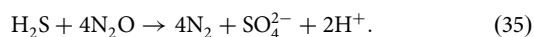
anaerobic ammonium oxidation via reduction of nitrite (known as anammox⁴⁰):



partial denitrification to nitrite and nitrous oxide via H₂S oxidation (PDNO):



and reduction of nitrous oxide to N₂ coupled with H₂S oxidation (RNO):



The concentration profile of organic matter is explicitly fixed in the model. The above reactions are largely fueled by H₂S and NH₄⁺ diffusing upward from the sediments, and O₂ and sinking organic matter from shallower waters. All metabolites are subject to vertical eddy diffusion, which varies across depth depending on the local buoyancy frequency⁴¹. At steady state, each metabolite's concentration thus satisfies the following PDE:

$$0 = \frac{\partial}{\partial z} \left[D(z) \frac{\partial U_j}{\partial z} \right] + \sum_{r=1}^6 \mathbb{S}_{jr} R_r(\mathbf{U}(z)), \quad (36)$$

where as before z denotes depth, D is the depth-dependent eddy diffusivity (m² · day⁻¹), \mathbb{S} is the stoichiometric matrix of the reactions and R_r is the rate of the r -th reaction (mol · L⁻¹ · d⁻¹). In contrast to the earlier SMTZ example, this model explicitly considers the population dynamics of microbial species catalyzing the reactions, with microbial growth being driven by the energy

released through the reactions. Each reaction rate R_r is thus proportional to the cell density of a unique microbial species catalyzing the reaction, henceforth denoted W_r and measured in cells per L. Per-cell reaction rates are assumed to follow first-order (mass action) or Monod kinetics in each substrate, with some reactions further inhibited by some metabolites:

$$R_r(\mathbf{U}) = W_r \cdot \beta_r \cdot F_r(\mathbf{U}) \cdot \prod_{j \in L_{r,1}} U_j \times \prod_{j \in L_{r,2}} \frac{U_j K_{r,j}}{U_j + K_{r,j}} \times \prod_{j \in I_r} \frac{K_{r,j}^*}{K_{r,j}^* + U_j}, \quad (37)$$

where $L_{r,1}$ and $L_{r,2}$ specify the substrates with first order and Monod order kinetics, respectively, for the r -th reaction, I_r specifies the inhibitors of the reaction, $K_{r,j}$ is the half-saturation constant for substrate j in reaction r , $K_{r,j}^*$ is the half-inhibition constant for inhibitor j in reaction r , β_r is the cell-specific affinity of the r -th reaction, and F_r is a *thermodynamic potential factor* that depends on metabolite concentrations and lowers the reaction rate when the latter is close to thermodynamic equilibrium⁴² Eq. 16. Note that here the affinity β_r is defined as the mass-action kinetic constant in the limit where all substrate and inhibitor concentrations approach zero. Cell death is modeled as an exponential decay process, and cells are subject to vertical eddy diffusion and sinking⁴³. Thus, at steady state each cell density W_r satisfies the PDE:

$$0 = \frac{\partial}{\partial z} \left[D(z) \frac{\partial W_r}{\partial z} \right] - \frac{\partial}{\partial z} (v_r \cdot W_r(z)) + R_r(\mathbf{U}) \frac{Y_r(\mathbf{U})}{M} - \delta_r W_r, \quad (38)$$

where δ_r is the constant exponential death rate for the r -th species (in units 1/day), Y_r is the biomass yield for that reaction (dry biomass produced per mole reaction flux), M is the average dry cell mass and v_r is the cell sinking speed. The yield Y_r is not a fixed parameter, but an empirically fitted linear function of the reaction's Gibbs free energy⁴⁴, and thus depends on metabolite concentrations and the reaction stoichiometry. Note that the model's dynamic variables include both \mathbf{U} and \mathbf{W} , that is, the system's state is defined by the tuple (\mathbf{U}, \mathbf{W}) .

Boundary conditions for metabolite concentrations at the top are all of fixed-value type, i.e., $U_j(a) = A_j$, where A_j is a constant. At the bottom, some metabolites have fixed-value conditions while others have zero flux conditions:

$$D(b) \frac{\partial U_j}{\partial z} \Big|_{z=b} = 0. \quad (39)$$

For cell densities, boundary conditions are either fixed values, or expressed in terms of fixed relative slopes, i.e.:

$$\frac{1}{W_r} \frac{\partial W_r}{\partial z} = \text{constant}. \quad (40)$$

Additional details, including parameter values, boundary conditions and the eddy diffusivity profile, can be found in the Supplement of²². An overview of the steady state predicted by the model for default parameter values, including metabolite concentration and cell density profiles across depth, is shown in Fig. 2. While microbial cells responsible for aerobic reactions (AEROM, AAO and ANO) are mostly abundant toward the upper end of the depth interval, anaerobic cells engaged in nitrogen reduction thrive at greater depths, causing the formation of a sharp sulfide-nitrate interface at around 130 m. For an extensive discussion of this steady state see ref. 22.

Focal parameters: Similarly to the earlier SMTZ example, let us focus on the model's rate-like parameters, i.e., the diffusivity D , the cell sinking speeds v_r , the reaction affinities β_r , and the per-capita cell death rates δ_r . A uniform rescaling of these parameters by a constant factor (while keeping \mathbf{U} and \mathbf{W} fixed) rescales the right hand side of the PDEs (Equations (36) and (38)) by that same factor, it rescales the zero-flux boundary conditions (Eq. (39)) by that factor, and leaves the fixed-value and fixed-relative slope

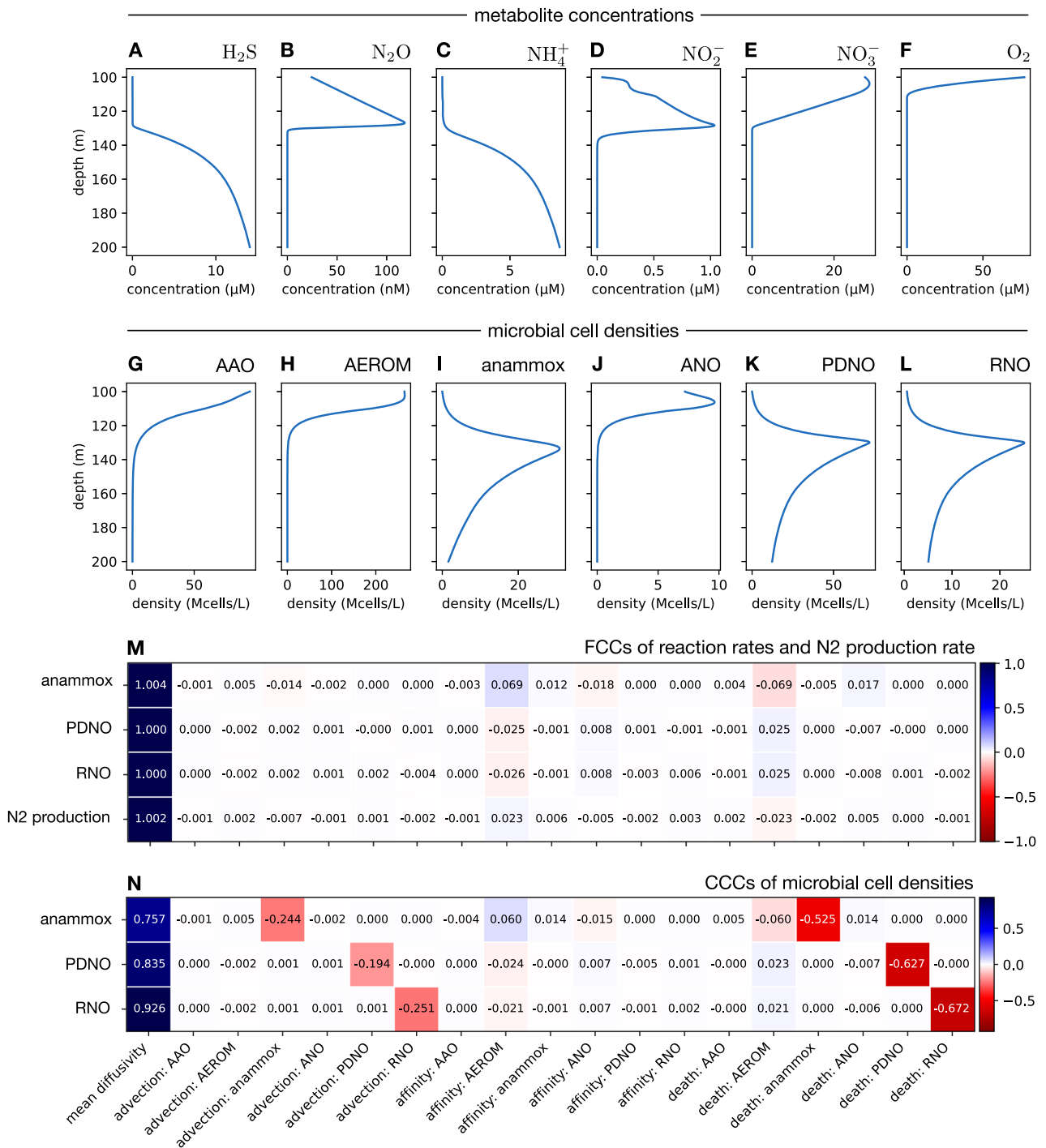


Fig. 2 | Saanich Inlet OMZ. A–F Steady state metabolite concentrations across the Saanich Inlet water column (0–600 cm), as predicted by the PDE model for February 2010. G–L Predicted steady state cell densities associated with each chemical

reaction. **M** FCCs for the mean rates of anammox, PDNO (partial denitrification to nitrous oxide), RNO (reduction of nitrous oxide using sulfide) and total N₂ production. **N** CCCs of mean microbial densities associated with these reactions.

boundary conditions (Eq. (40)) unchanged. Thus, this set of parameters satisfies the homogeneity condition for F_w in Eq. (9) and consequently the invariance condition for steady states (Eq. (7)). Uniformly rescaling these parameters (while keeping U and W fixed) also rescales each reaction rate R_i by the same factor, and thus reaction rates (and their averages across space) satisfy the homogeneity condition for fluxes in Eq. (13). A similar conclusion holds for the production and consumption rates of metabolites, as well as for microbial cell generation and death rates. Following the earlier discussion on grouping parameters, for MCA it is simpler to consider the average diffusivity $\bar{D} := \frac{1}{b-a} \int_a^b D(z) dz$, while keeping the location-

dependent normalized diffusivity $d(z) := D(z)/\bar{D}$ fixed. Thus, the vector of focal parameters is:

$$\mathbf{p} = (\bar{D}, v_{\text{AEROM}}, \dots, v_{\text{RNO}}, \beta_{\text{AEROM}}, \dots, \beta_{\text{RNO}}, \delta_{\text{AEROM}}, \dots, \delta_{\text{RNO}}). \tag{41}$$

Control coefficients: While the model makes predictions about many different fluxes and coupled reactions, for MCA I henceforth focus on those directly involved in fixed nitrogen loss. Specifically, I consider the FCCs of the mean anammox, PDNO, and RNO reaction rates, the FCCs of the mean

rate of N_2 production, the CCCs of the mean cell densities associated with anammox, PDNO, and RNO (Fig. 2M, N), as well as fluxes of nitrogen compounds across the top and bottom boundaries (100 m and 200 m depth). In contrast to the earlier SMTZ example, a small number of FCCs is actually negative, indicating that some focal parameters have a negative impact on process rates. The most negative FCC (-0.069) was obtained for anammox with respect to the per-capita death rate of AEROM cells. A likely explanation is that a higher mortality of AEROM cells reduces AEROM cell densities and thus AEROM reaction rates, in turn increasing the amount of oxygen that is available for aerobic ammonia oxidation and aerobic nitrite oxidation, both of which compete for nitrogen substrates with anammox, thus in turn reducing anammox rates. That said, negative FCCs are all relatively weak (i.e., close to zero), and thus — due to the FCC summation theorem — one can still approximately interpret the remaining non-negative FCCs as fractions of overall control. By far the strongest FCCs are those associated with the mean diffusivity (\bar{D}), attaining values close to 1 in all cases. This suggests that eddy diffusion (turbulent mixing) was by far the most important modeled rate-limiting process for fixed nitrogen loss in Saanich Inlet during the considered time period. In contrast, FCCs associated with reaction affinities (β_r) are all close to zero, which implies that changes in the considered reaction affinities would only have a minimal impact on fixed nitrogen loss. Similar results are also obtained when focusing on the mean reaction rates around the redox transition zone (120–140 m, Fig. S2A). This suggests that for purposes of predicting overall fixed nitrogen loss rates in oxygen minimum zones it is more important to accurately characterize hydrodynamic mixing processes than the kinetics of supply-limited reactions. It should be noted that in this model the cycling of organic matter is not modeled fully mechanistically, since the depth-profile of organic matter was fixed and the production kinetics of organic matter are not considered at all. Organic matter remineralization, especially extracellular hydrolysis of organic macromolecules, is often considered the rate-limiting step in microbial communities^{45,46}, and in the present analysis the affinity and death rate of AEROM did have the strongest control on N_2 production among all reactions (Fig. 2). Further investigations are thus necessary to elucidate the control exerted by carbon cycling processes on fixed nitrogen loss.

Interestingly, the distribution of FCCs across parameters becomes more complex when one considers fluxes of nitrogen compounds (N_2 , N_2O , NO_2^- , NO_3^- and NH_4^+) across individual boundaries (Fig. S2C). While the flux of NH_4^+ across the bottom boundary is largely controlled by diffusivity (FCC 0.998, all other FCCs close to zero), for all other examined compounds FCCs cover a variety of values, including values far from 0 and 1 and even strongly negative values. For example, for N_2 flux across the top boundary, FCCs range from -0.65 and -0.58 with respect to the affinities of anammox and ANO, respectively, to 0.58 with respect to the affinity of AAO and up to 1.14 with respect to the diffusivity. A similarly complex partitioning is seen for N_2 flux across the bottom boundary. This suggests that the partitioning of N_2 release across the top and bottom boundary depends in complex ways on both transport and reaction kinetics, despite the fact that their sum (equal to total N_2 production) is almost entirely controlled by diffusivity alone (Fig. 2M).

CCCs for mean cell densities display a somewhat more diversified dependency (Fig. 2N). While CCCs associated with diffusivity (leftmost column in Fig. 2N) are still the strongest by magnitude, substantial control is also exerted by per-capita death rates (δ_r) and to a lesser extent by cell sinking speeds (v_r). On the other hand, reaction affinities exert almost no control on cell densities. These observations may come as no surprise, since steady state cell densities results from a balance between processes that add cells (mainly chemical reactions, whose rates are insensitive to affinities) and processes that remove cells (i.e., sinking and death).

Comparison to other common sensitivity analyses

It is worth noting where MCA stands in relation to other types of sensitivity analysis. Since FCCs and CCCs are based on partial derivatives of model responses with respect to focal parameters, MCA constitutes a local

sensitivity analysis, that is, it only informs about the sensitivity of the system to small parameter changes. This contrasts MCA with global sensitivity analyses, for example those that “sweep” a wide range of parameter values⁴⁷ and Monte Carlo methods⁴⁸ (for a detailed comparison between local and global sensitivity analyses see refs. 49,50). In fact, FCCs and CCCs are a special case of normalized local sensitivity coefficients^{22,27}, focused on specific types of observables (fluxes and concentrations) and focal parameters that control the system’s pace. The deliberate examination of a subset of pace-setting focal parameters, and the recognition of system responses with particular sensitivity properties (here, termed “fluxes” and “concentrations”), gives MCA additional structure and interpretability, including summation theorems that relate the sensitivity coefficients to each other, and the interpretation of FCCs as fractional contributions to flux control.

Conclusions

Classical MCA has been an invaluable tool in understanding the controls of cellular biochemical reaction networks modeled via ordinary differential equations. The generalization presented here covers a much wider range of reactive systems, such as microbial communities coupled to redox chemistry in water columns, sediments or bioreactors, elemental cycles at regional or planetary scales, and even ecological food webs (Supplementary Discussion 1). Mathematically, this generalized MCA can accommodate a broad range of model structures, including nearly arbitrary combinations of ordinary differential, partial differential, integral, and algebraic equations. Indeed, the two critical assumptions made are the invariance of steady states (Eq. (7)) and the 1-homogeneity of fluxes (Eq. (13)) to a uniform rescaling of the focal parameters, regardless of the precise model structure.

The focal parameters defined here present an intuitive generalization of the enzyme activities considered in classical MCA. As illustrated through multiple examples, focal parameters will often correspond to the rate-like parameters (and inverses of time-like parameters) in a model, which define the time scales of various processes and the “pace” of a system’s dynamics. In that sense, control coefficients formalize the dependency of a system’s emergent properties on the time scales of individual constituent processes, such as chemical reactions, microbial population growth or death, diffusive and advective transport, outgassing at water-air interfaces, or hydraulic renewal in bioreactors. The concentration and flux control summation theorems, in turn, reveal fundamental relationships between control coefficients; for example, since all CCCs must sum to zero, negative CCCs inevitably imply the existence of positive CCCs as well, and increasing some CCCs will necessarily decrease other CCCs.

In both of the detailed simulation examples discussed, the sulfate-methane transition zone in Black Sea sediments and a seasonal oxygen minimum zone in Saanich Inlet at quasi-steady state, physical transport processes across space were found to exert by far the greatest control on the fluxes of interest. This suggests that greater emphasis should be put on characterizing the transport processes in such systems, compared to the chemical and microbial kinetics. These examples demonstrate the great potential that MCA has for determining the rate-limiting processes in natural and engineered reactive systems.

While I focused on systems at steady state, it is expected that MCA as presented here is also approximately applicable to systems at quasi-steady state. Here, quasi-steady state is taken to mean that the system quickly converges to and closely follows a state \bar{U} that is solely determined by the model parameters, with the latter either being constant or changing over much longer time scales than the time it takes for the system to converge to \bar{U} . In that case, predicted concentrations and fluxes, as well as their control coefficients, would be time-dependent quantities determined by the current parameter values. How far from steady state the theory presented here starts to fail remains an open and complex question. It might also be possible to rigorously generalize MCA to systems far from steady state, albeit at the risk of complicating interpretations. Indeed, classical MCA has been generalized to time-dependent biochemical networks^{30,32}, but its adoption has been limited compared to steady state MCA, partly due to the added complexity.

The predictive power of classical MCA and its potential to yield practical insight into cell metabolism have been confirmed through numerous experiments and successful bioengineering outcomes guided by MCA^{18,19}. By analogy, I anticipate that the potential of the generalized MCA presented here will become further apparent through successful predictions of geochemical/ecological flux changes in response to specific environmental shifts, as well as future eco- and geo-engineering successes guided by MCA.

Methods

Additional details on the structure, parameterization and simulation of the Black Sea SMTZ model are provided in Supplementary Discussion 2. The Saanich Inlet oxygen minimum zone model is described in detail in ref. 22.

Data availability

No data were generated or analyzed by this project.

Code availability

The simulation code for the Black Sea and Saanich Inlet models is freely available at: <http://www.loucalab.com/archive/MetabolicControlAnalysis>.

Received: 29 August 2024; Accepted: 12 February 2025;

Published online: 28 February 2025

References

- Falkowski, P. G., Fenchel, T. & Delong, E. F. The microbial engines that drive Earth's biogeochemical cycles. *Science* **320**, 1034–1039 (2008).
- DeVries, T. The ocean carbon cycle. *Annu. Rev. Environ. Resour.* **47**, 317–341 (2022).
- Decker, K. L. M. et al. Mathematical simulation of the diel O₂, S₂, and C biogeochemistry of a hypersaline microbial mat. *FEMS Microbiol. Ecol.* **52**, 377–395 (2005).
- Amarasekare, P. Spatial dynamics of foodwebs. *Annu. Rev. Ecol. Evol. Syst.* **39**, 479–500 (2008).
- Daims, H., Taylor, M. W. & Wagner, M. Wastewater treatment: a model system for microbial ecology. *Trends Biotechnol.* **24**, 483–489 (2006).
- Jin, Q. & Bethke, C. M. Predicting the rate of microbial respiration in geochemical environments. *Geochim. et. Cosmochim. Acta* **69**, 1133–1143 (2005).
- Jin, Q., Roden, E. E. & Giska, J. R. Geomicrobial kinetics: Extrapolating laboratory studies to natural environments. *Geomicrobiol. J.* **30**, 173–185 (2013).
- Louca, S. et al. Circumventing kinetics in biogeochemical modeling. *Proc. Natl Acad. Sci.* **116**, 11329–11338 (2019).
- Louca, S., Taylor, G. T., Astor, Y. M., Buck, K. & Muller-Karger, F. E. Transport-limited reactions in microbial systems. *Environ. Microbiol.* **25**, 268–282 (2022).
- Scheibe, T. D., Tartakovsky, A. M., Tartakovsky, D. M., Redden, G. D. & Meakin, P. Hybrid numerical methods for multiscale simulations of subsurface biogeochemical processes. *J. Phys.: Conf. Ser.* **78**, 012063 (2007).
- Molins, S. & Knabner, P. Multiscale approaches in reactive transport modeling. *Rev. Mineral. Geochem.* **85**, 27–48 (2019).
- Qu, Z., Garfinkel, A., Weiss, J. N. & Nivala, M. Multi-scale modeling in biology: How to bridge the gaps between scales? *Prog. Biophys. Mol. Biol.* **107**, 21–31 (2011).
- Wang, B., Wang, Z., Chen, T. & Zhao, X. Development of novel bioreactor control systems based on smart sensors and actuators. *Front. Bioeng. Biotechnol.* **8**, 7 (2020).
- Giersch, C. Control analysis of metabolic networks. *Eur. J. Biochem.* **174**, 509–513 (1988).
- Kacser, H., Burns, J. A., Kacser, H. & Fell, D. The control of flux. *Biochem. Soc. Trans.* **23**, 341–366 (1995).
- Hofmeyr, J. H. S. Metabolic control analysis in a nutshell. *Proc. 2nd Int. Conf. Syst. Biol.* **2**, 291–300 (2001).
- Morandini, P. Rethinking metabolic control. *Plant Sci.* **176**, 441–451 (2009).
- Cascante, M. et al. Metabolic control analysis in drug discovery and disease. *Nat. Biotechnol.* **20**, 243–249 (2002).
- Moreno-Sánchez, R., Saavedra, E., Rodríguez-Enríquez, S. & Olin-Sandoval, V. Metabolic control analysis: A tool for designing strategies to manipulate metabolic pathways. *BioMed. Res. Int.* **2008**, 597913 (2008).
- Jørgensen, B. B., Böttcher, M. E., Lüschen, H., Neretin, L. N. & Volkov, I. I. Anaerobic methane oxidation and a deep H₂S sink generate isotopically heavy sulfides in Black Sea sediments. *Geochim. et. Cosmochim. Acta* **68**, 2095–2118 (2004).
- Egger, M. et al. Anaerobic oxidation of methane alters sediment records of sulfur, iron and phosphorus in the Black Sea. *Biogeosciences* **13**, 5333–5355 (2016).
- Louca, S. et al. Integrating biogeochemistry with multiomic sequence information in a model oxygen minimum zone. *Proc. Natl Acad. Sci.* **113**, E5925–E5933 (2016).
- Hawley, A. K. et al. A compendium of multi-omic sequence information from the Saanich Inlet water column. *Nat. Sci. Data* **4**, 170160 EP (2017).
- Torres-Beltrán, M. et al. A compendium of geochemical information from the Saanich Inlet water column. *Nat. Sci. Data* **4**, 170159 EP (2017).
- Shen, W. *An Introduction To Numerical Computation* (World Scientific Publishing Company, 2019), 2 edn.
- Jung, S. M. & Min, S. Stability of the diffusion equation with a source. *J. Funct. Spaces* **2018**, 1216901 (2018).
- Christopher Frey, H. & Patil, S. R. Identification and review of sensitivity analysis methods. *Risk Anal.* **22**, 553–578 (2002).
- Dobbs, D. E. On the smoothness condition in Euler's theorem on homogeneous functions. *Int. J. Math. Educ. Sci. Technol.* **49**, 1250–1259 (2018).
- Pir, P. et al. The genetic control of growth rate: a systems biology study in yeast. *BMC Syst. Biol.* **6**, 4 (2012).
- Acerenza, L., Sauro, H. M. & Kacser, H. Control analysis of time-dependent metabolic systems. *J. Theor. Biol.* **137**, 423–444 (1989).
- Conradie, R., Westerhoff, H. V., Rohwer, J. M., Hofmeyr, J. H. & Snoep, J. L. Summation theorems for flux and concentration control coefficients of dynamic systems. *IEE Proc. - Syst. Biol.* **153**, 314–317 (2006).
- Cornish-Bowden, A. & Cárdenas, M.L. *Control of metabolic processes*, vol. 190 (Springer Science & Business Media, 2013).
- Reed, D. C., Algar, C. K., Huber, J. A. & Dick, G. J. Gene-centric approach to integrating environmental genomics and biogeochemical models. *Proc. Natl Acad. Sci.* **111**, 1879–1884 (2014).
- Li, X. N., Taylor, G. T., Astor, Y., Varela, R. & Scranton, M. I. The conundrum between chemoautotrophic production and reductant and oxidant supply: A case study from the Cariaco Basin. *Deep Sea Res. Part I: Oceanogr. Res. Pap.* **61**, 1–10 (2012).
- Knittel, K. & Boetius, A. Anaerobic oxidation of methane: Progress with an unknown process. *Annu. Rev. Microbiol.* **63**, 311–334 (2009).
- Smith, S. L., Yamanaka, Y., Pahlow, M. & Oschlies, A. Optimal uptake kinetics: physiological acclimation explains the pattern of nitrate uptake by phytoplankton in the ocean. *Mar. Ecol. Prog. Ser.* **384**, 1–12 (2009).
- Aksnes, D. L. & Cao, F. J. Inherent and apparent traits in microbial nutrient uptake. *Mar. Ecol. Prog. Ser.* **440**, 41–51 (2011).
- Ulloa, O., Canfield, D. E., DeLong, E. F., Letelier, R. M. & Stewart, F. J. Microbial oceanography of anoxic oxygen minimum zones. *Proc. Natl Acad. Sci.* **109**, 15996–16003 (2012).
- Zehr, J. P. & Kudela, R. M. Nitrogen cycle of the open ocean: from genes to ecosystems. *Annu. Rev. Mar. Sci.* **3**, 197–225 (2011).

40. Dalsgaard, T., Thamdrup, B. & Canfield, D. E. Anaerobic ammonium oxidation (anammox) in the marine environment. *Res. Microbiol.* **156**, 457–464 (2005).
41. Gargett, A. E. Vertical eddy diffusivity in the ocean interior. *J. Mar. Res.* **42**, 359–393 (1984).
42. LaRowe, D. E., Dale, A. W., Amend, J. P. & Van Cappellen, P. Thermodynamic limitations on microbially catalyzed reaction rates. *Geochim. et. Cosmochim. Acta* **90**, 96–109 (2012).
43. Fennel, K. et al. Nitrogen cycling in the Middle Atlantic Bight: Results from a three-dimensional model and implications for the North Atlantic nitrogen budget. *Glob. Biogeochem. Cycles* **20**, GB3007 (2006).
44. Roden, E. E. & Jin, Q. Thermodynamics of microbial growth coupled to metabolism of glucose, ethanol, short-chain organic acids, and hydrogen. *Appl. Environ. Microbiol.* **77**, 1907–1909 (2011).
45. Arndt, S. et al. Quantifying the degradation of organic matter in marine sediments: A review and synthesis. *Earth-Sci. Rev.* **123**, 53–86 (2013).
46. Enke, T. N., Leventhal, G. E., Metzger, M., Saavedra, J. & Cordero, O. X. Microscale ecology regulates particulate organic matter turnover in model marine microbial communities. *Nat. Commun.* **9**, 2743 (2018).
47. Kriest, I., Oschlies, A. & Khatiwala, S. Sensitivity analysis of simple global marine biogeochemical models. *Glob. Biogeochem. Cycles* **26**, GB2029 (2012).
48. Louca, S., Lampo, M. & Doebeli, M. Assessing host extinction risk following exposure to *Batrachochytrium dendrobatidis*. *Proc. R. Soc. B* **281**, 20132783 (2014).
49. Razavi, S. & Gupta, H. V. What do we mean by sensitivity analysis? the need for comprehensive characterization of “global” sensitivity in earth and environmental systems models. *Water Resour. Res.* **51**, 3070–3092 (2015).
50. Iooss, B. & Lemaitre, P. *A review on global sensitivity analysis methods*, 101–122 (Springer US, Boston, MA, 2015).

Acknowledgements

SL was supported by a Simons Foundation early career investigator award.

Author contributions

SL conceived the project, performed all analyses and wrote the manuscript.

Competing interests

The author declares no competing interests.

Additional information

Supplementary information The online version contains supplementary material available at <https://doi.org/10.1038/s43247-025-02135-1>.

Correspondence and requests for materials should be addressed to Stilianos Louca.

Peer review information *Communications Earth & Environment* thanks and the other, anonymous, reviewer(s) for their contribution to the peer review of this work. Primary Handling Editors: D’Arcy Meyer-Dombard and Alice Drinkwater. [A peer review file is available].

Reprints and permissions information is available at <http://www.nature.com/reprints>

Publisher’s note Springer Nature remains neutral with regard to jurisdictional claims in published maps and institutional affiliations.

Open Access This article is licensed under a Creative Commons Attribution 4.0 International License, which permits use, sharing, adaptation, distribution and reproduction in any medium or format, as long as you give appropriate credit to the original author(s) and the source, provide a link to the Creative Commons licence, and indicate if changes were made. The images or other third party material in this article are included in the article’s Creative Commons licence, unless indicated otherwise in a credit line to the material. If material is not included in the article’s Creative Commons licence and your intended use is not permitted by statutory regulation or exceeds the permitted use, you will need to obtain permission directly from the copyright holder. To view a copy of this licence, visit <http://creativecommons.org/licenses/by/4.0/>.

© The Author(s) 2025

Metabolic control analysis of biogeochemical systems - Supplementary Information -

Stilianos Louca^{1,2,*}

¹Department of Biology, University of Oregon, Eugene, USA

²Institute of Ecology and Evolution, University of Oregon, Eugene, USA

*Corresponding author

S.1 Supplementary Discussion 1: Additional examples

In this section I present various reactive models that meet the assumptions of the generalized MCA discussed in the main article. I do not present any simulation results - rather, the goal is to demonstrate how the model's notation fits into the notation used in the main article, how to choose the focal parameters \mathbf{p} , and how to verify the generalized MCA assumptions.

S.1.1 Biochemical reaction networks (classical MCA)

In this section I briefly discuss the classical use case of MCA, that is, biochemical reaction networks without explicit spatial structure modeled by ordinary differential equations. While such models have been discussed many times before in the context of classical MCA [1–6], they are included here in order to further clarify the connection of the generalized concepts discussed in the main article to classical MCA. The typical model tracks the concentrations of m metabolites, U_1, \dots, U_m , in a well-mixed system, subject to chemical transformations by enzymatic reactions proceeding at rates R_1, \dots, R_n . Note that \mathbf{U} only includes metabolites with dynamic concentrations, while metabolites with fixed (externally buffered) concentrations are regarded as model parameters. Stoichiometric coefficients of reactions are combined in a single stoichiometric matrix, $\mathbb{S} \in \mathbb{R}^{(m+k) \times n}$, with the top m rows of \mathbb{S} (henceforth \mathbb{S}^d) corresponding to dynamic metabolites and the bottom k rows of \mathbb{S} (henceforth \mathbb{S}^b) corresponding to buffered metabolites. The rate of change of dynamic metabolites is equal to their net rate of production, i.e.:

$$\frac{d\mathbf{U}}{dt} = \mathbb{S}^d \cdot \mathbf{R}. \quad (1)$$

While some metabolites may be buffered, their net production rates due to reactions may still be of interest and can be computed as $\mathbb{S}^b \cdot \mathbf{R}$. In classical MCA, it is assumed that each reaction is driven by a distinct enzyme, and that the reaction rate depends linearly on the activity of that enzyme:

$$R_i = E_i \cdot f_i(\mathbf{U}), \quad (2)$$

where each f_i is an arbitrary function of \mathbf{U} and E_i is the fixed enzyme activity. In particular, apart from its dependency on substrate concentrations, each reaction is assumed to be limited solely by the availability of enzymes. Just like the fixed concentrations of any buffered metabolites, so the E_1, \dots, E_n are treated as model parameters (albeit, of particular interest). I henceforth write $R_i(\mathbf{U}, \mathbf{E})$ to emphasize the dependency of reaction rates on \mathbf{U} as well as \mathbf{E} . The steady state $\bar{\mathbf{U}}$ is defined as the solution to $\mathbb{S}^d \cdot \mathbf{R}(\bar{\mathbf{U}}, \mathbf{E}) = 0$. Thus, following the notation of the main article:

$$F_\omega(\mathbf{U}, \mathbf{E}) = \sum_{i=1}^n \mathbb{S}_{\omega,i}^d \cdot R_i(\mathbf{U}, \mathbf{E}), \quad (3)$$

where ω takes values in $\Omega := \{1, \dots, m\}$. Each F_ω is positively homogeneous in \mathbf{E} , that is:

$$F_\omega(\mathbf{U}, \alpha \mathbf{E}) = \sum_{i=1}^n \mathbb{S}_{\omega,i}^d \cdot R_i(\mathbf{U}; \alpha \mathbf{E}) = \sum_{i=1}^n \mathbb{S}_{\omega,i}^d \cdot \alpha R_i(\mathbf{U}; \mathbf{E}) = \alpha F_\omega(\mathbf{U}, \mathbf{E}), \quad (4)$$

for any $\alpha > 0$. Following the discussion in the main article, this means that steady states are invariant to a uniform rescaling of \mathbf{E} (Eq. 7). Thus, \mathbf{E} satisfies the MCA conditions stated for focal parameters. Since each R_i is positively 1-homogeneous in \mathbf{E} , i.e., $R_i(\mathbf{U}, \alpha \mathbf{E}) = \alpha R_i(\mathbf{U}, \mathbf{E})$ for any $\alpha > 0$, each reaction rate satisfies the homogeneity assumption for fluxes stated in the main article (Eq. 13). The same also holds for the net production rate of any metabolite, dynamic and buffered. Control analysis of reaction rates with

respect to the focal parameters \mathbf{E} corresponds exactly to classical MCA. Often, the focus is on the production or consumption rate of specific metabolites, such as a drug or toxin. It is worth mentioning that classical MCA includes additional concepts such as *elasticity coefficients*, which encode the sensitivity of \mathbf{R} to small changes in \mathbf{U} , and which are elegantly related to control coefficients via so called *connectivity theorems* [4, 7]. However, these theorems rely heavily on the specific mathematical structure of biochemical reaction networks (i.e., Eq. 1), and hence elasticity coefficients are less meaningful (and may even be impossible to define) for many of the systems discussed in this article.

S.1.2 Predator prey model

In this section I exemplify MCA on a predator-prey differential equation model, known as Rosenzweig-MacArthur model and widely used in ecology [8–10]. The model tracks the densities of a prey (N) and a predator (P) over time, according to the following ordinary differential equations:

$$\begin{aligned}\frac{dN}{dt} &= \rho N - \beta N^2 - \frac{\gamma NP}{D + N}, \\ \frac{dP}{dt} &= Y \frac{\gamma NP}{D + N} - \frac{P}{\tau}.\end{aligned}\tag{5}$$

Here, ρ is the prey's maximum per-capita population growth rate, β is the per-capita effect of an additional prey competitor (the carrying capacity is $K = \rho/\beta$), γ is the maximum killing rate achievable by a single predator (i.e., as N tends to ∞), D is the half-saturation constant accounting for a saturation of prey killing rates at high prey densities, Y is the conversion efficiency or yield and τ is the predator's expected life time in the absence of prey. Depending on the parameter values, the model exhibits either damped oscillations converging to a locally stable steady state in which both predator and prey coexist, or limit cycle (sustained) oscillations. I henceforth assume that parameter values are such that a non-trivial stable steady state exists, i.e., where both prey and predator coexist stably at constant densities.

The system's state at any time is fully specified by the tuple (N, P) , henceforth denoted \mathbf{U} . The state states \mathbf{U} are defined as the solutions to:

$$\begin{aligned}\rho N - \beta N^2 - \frac{\gamma NP}{D + N} &= 0, \\ Y \frac{\gamma NP}{D + N} - \frac{P}{\tau} &= 0.\end{aligned}\tag{6}$$

Hence, in the notation introduced in the main article (Eq. 4) we have:

$$\begin{aligned}F_1(\mathbf{U}, \mathbf{p}) &= \rho N - \beta N^2 - \frac{\gamma NP}{D + N}, \\ F_2(\mathbf{U}, \mathbf{p}) &= Y \frac{\gamma NP}{D + N} - \frac{P}{\tau},\end{aligned}\tag{7}$$

where the set of focal parameters \mathbf{p} is yet to be determined. In order to satisfy the invariance condition for steady states (Eq. 7), it suffices to select focal parameters satisfying the homogeneity condition for F_1 and F_2 , that is, such that $F_\omega(\mathbf{U}, \alpha \mathbf{p}) = \alpha^\kappa F_\omega(\mathbf{U}, \mathbf{p})$ for some fixed $\kappa \in \mathbb{R}$ and for all \mathbf{p} , \mathbf{U} and all $\alpha > 0$.

Following the general guidance discussed in the main article, as a possible set of focal parameters I consider all rate-like parameters and the inverses of all time-like parameters, that is, ρ, β, γ and $\delta := 1/\tau$. Indeed, multiplying each of ρ, β, γ and δ with a factor α (while keeping \mathbf{U} unchanged) rescales F_1 and F_2 by that same factor (i.e., $\kappa = 1$). These parameters essentially determine the pace of the system. Note that additionally including any of the remaining model parameters, such as Y or D , as focal would violate the homogeneity

condition for F_ω . For example, the set $\rho, \beta, \gamma, \delta, Y$ no longer satisfies the homogeneity condition, since:

$$F_2(\mathbf{U}, \alpha\rho, \alpha\beta, \alpha\gamma, \alpha\delta, \alpha Y) = \alpha^2 \cdot Y \frac{\gamma NP}{D + N} - \alpha \cdot \frac{P}{\tau}. \quad (8)$$

Due to the varying polynomial powers of the factor α on the right hand side of Eq. (8), there exists no single κ such that the above is equal to $\alpha^\kappa F_2(\mathbf{U}, \rho, \beta, \gamma, \delta, Y)$ for all α .

Note that both N and P can be considered ‘‘concentrations’’ following the MCA terminology introduced in the main article, so their CCCs will satisfy the concentration control summation theorem. One can also readily identify various ‘‘fluxes’’ in the system, for example:

$$\begin{aligned} \text{prey births:} \quad J_1 &:= \rho N \\ \text{prey killings:} \quad J_2 &:= \frac{\gamma NP}{D + N} \\ \text{predator deaths:} \quad J_3 &:= \delta P \end{aligned} \quad (9)$$

Indeed, uniformly rescaling the focal parameters (while holding \mathbf{U} constant) will rescale each of the above quantities by the same factor, thus satisfying the homogeneity assumption for fluxes in Eq. (13). Consequently, following the flux control summation theorem, the FCCs of each of these fluxes associated with the focal parameters will always sum to 1.

S.1.3 Carbon cycle overlaid on an ocean general circulation model

In this example I consider a 3-dimensional global ocean carbon cycle model, tracking the distributions of dissolved inorganic carbon (DIC), alkalinity, phosphate (PO_4^{3-}) and dissolved organic phosphorous (DOP) in the ocean as well as the total CO_2 concentration in the atmosphere. The model is a simplified self-contained version of a larger previously published model [11], which was built for climatic predictions on top of the MIT ocean general circulation model (MITgcm; [12, 13]). Unless otherwise stated, parameter values are given in [11, Table 2]. The model’s dynamic variables are DIC concentration (U_{DIC}), alkalinity (U_{alk}), phosphate concentration (U_{phs}) and DOP concentration (U_{DOP}) across the ocean as well as the CO_2 concentration in the atmosphere (U_{CO_2}). The first 4 of these variables vary across space, while the latter is scalar-valued, since for simplicity I assume that the atmosphere is well mixed. The dynamics of these variables are influenced by ocean currents, temperature and salinity, but are assumed to have negligible influence on the latter. Thus, the system evolves on an advective/diffusive backdrop and a given temperature and salinity field, which have been precomputed using the physical general ocean circulation model and are henceforth considered as given parameters. While a priori ocean currents, temperature and salinity depend on both time and space, we henceforth focus on steady states and thus assume that these quantities have all been averaged over time, so that they only depend on space. Horizontal coordinates are denoted x, y and depth is denoted z .

The atmospheric CO_2 concentration is assumed to be solely affected by gas exchange with the ocean, i.e., the model ignores sources and sinks of CO_2 within the atmosphere and on land. The net upward flux rate of CO_2 through the water-air interface at any given lateral location (x, y) is given by:

$$F_{\text{CO}_2}(x, y) = \kappa_w \cdot [C(U_{\text{DIC}}(x, y, 0), U_{\text{alk}}(x, y, 0), U_{\text{phs}}(x, y, 0)) - H_{\text{cc}} \cdot U_{\text{CO}_2}], \quad (10)$$

where H_{cc} is the unitless (concentration/concentration) Henry solubility constant [14], κ_w is a gas transfer coefficient (measured in distance/time; [15]), and C is a function that specifies the local CO_2 concentration in surface waters depending on DIC, alkalinity and phosphate as well as on temperature and salinity [11]. Note that κ_w generally depends on local temperature, wave intensity and wind speed, however for simplicity

we assume that both κ_w and H_{cc} are constants. Thus, U_{CO_2} follows the differential equation:

$$\frac{dU_{CO_2}}{dt} = \frac{1}{h} \cdot \int \int F_{CO_2}(x, y) dx dy, \quad (11)$$

where the 2-dimensional integral covers the entire ocean surface and h is the effective height of the atmosphere box. The variables U_{DIC} , U_{alk} , U_{phs} and U_{DOP} satisfy the following PDE:

$$\frac{\partial U_j}{\partial t} = -\nabla \cdot (\mathbf{v}U_j) + \nabla \cdot (\mathbb{D}\nabla U_j) + S_j, \quad (12)$$

where \mathbf{v} is the advection field and \mathbb{D} the diffusion tensor obtained from the physical ocean circulation model, and each S_j is a source term representing production/consumption due to biological and chemical processes. Since we are mainly interested in steady states, we henceforth impose the conditions that $\partial U_j / \partial t = 0$. The source terms are given by:

$$\begin{aligned} S_{DIC} &= r_{C:P} S_{phs} + J_{Ca}, \\ S_{alk} &= -r_{N:P} S_{phs} + 2J_{Ca}, \\ S_{phs} &= -J_{prod} + a_{remin}(1 - f_{DOP})J_{prod}L \frac{z_c^{a_{remin}}}{z^{1+a_{remin}}} + \kappa_{remin}U_{DOP}, \\ S_{DOP} &= f_{DOP}J_{prod} - \kappa_{remin}U_{DOP}, \end{aligned} \quad (13)$$

where J_{prod} is net biological productivity in terms of organic phosphorus production:

$$J_{prod}(x, y, z) = \alpha_{prod} \cdot \frac{I(z)}{I(z) + \kappa_I} \cdot \frac{U_{phs}(x, y, z)}{U_{phs}(x, y, z) + \kappa_{phs}}, \quad (14)$$

and I represents depth-dependent photosynthetically available light:

$$I(x, y, z) = I_0(x, y) \cdot e^{-z/\delta_I}, \quad (15)$$

and J_{Ca} represents export of plankton-generated calcium carbonate to depth:

$$\begin{aligned} J_{Ca}(x, y, z) &= -Rr_{C:P}(1 - f_{DOP})J_{prod}(x, y, z) \\ &\quad - Rr_{C:P}(1 - f_{DOP})J_{prod}(x, y, z) \frac{L}{\delta_{Ca}} e^{-(z-z_c)/\delta_{Ca}}. \end{aligned} \quad (16)$$

In the above equations, $I_0(x, y)$ is the location-dependent average photosynthetically available light intensity at depth 0 (previously estimated for example from annual average weather data, or using a physical atmospheric model), κ_I and κ_{phs} are half-saturation constants, α_{prod} is the maximum possible biological production rate (a constant), δ_I is the constant depth-scale of light attenuation, δ_{Ca} is the constant depth-scale of $CaCO_3$ remineralization, $r_{C:P}$ is the constant carbon:phosphorus Redfield ratio, $r_{N:P}$ is the constant nitrogen:phosphorus Redfield ratio, R is a constant ‘‘rain-ratio’’ sensu Yamanaka and Tajika [16], κ_{remin} is the reaction affinity (mass-action coefficient) for DOP remineralization, a_{remin} is a constant unitless power-law exponent for remineralization of sinking particulate organic phosphate, f_{DOP} is the constant fraction of produced organic phosphorus that remains suspended in the water column as DOP, z_c is the depth of base of each layer where production occurs, and L is a constant layer width. Note that the full model by Dutkiewicz *et al.* [11] also accounts for freshwater fluxes at the ocean surface (e.g., due to precipitation), which are omitted here for simplicity. Boundary conditions for U_{DIC} , U_{alk} , U_{phs} and U_{DOP} are zero-flux everywhere,

except for U_{DIC} at the ocean surface, where the boundary influx is set to $-F_{\text{CO}_2}$:

$$\mathbf{n} \cdot (\mathbf{v}U_{\text{DIC}} - \mathbb{D}\nabla U_{\text{DIC}}) = \begin{cases} -F_{\text{CO}_2} & : \text{at ocean surface} \\ 0 & : \text{anywhere else} \end{cases}, \quad (17)$$

$$\mathbf{n} \cdot (\mathbf{v}U_j - \mathbb{D}\nabla U_j) = 0 \quad \text{for } j \in \{\text{alk, phs, DOP}\},$$

where \mathbf{n} is the inward unit normal vector at the boundary. For an explanation of the various processes modeled above see [11, Section 2.2.3].

MCA: Following the notation in the main article, the various F_ω correspond to the right hand side of the PDE (12) separately for each point in space and for each $j = \{\text{DIC, alk, phs, DOP}\}$, and to the right hand side of the differential equation (11). As in the previous examples, as focal parameters for MCA one may consider all rate-like parameters, that is, \mathbf{v} , \mathbb{D} , κ_w , α_{prod} , κ_{remin} . These parameters dictate the time scales of the four coupled processes in the model: hydrodynamic transport in the ocean (\mathbf{v} and \mathbb{D}), gas exchange with the atmosphere (κ_w), generation of organic matter (α_{prod}) and remineralization of organic matter (κ_{remin}), and essentially determine the ‘‘pace’’ of the system’s dynamics. Rescaling all of these parameters by the same factor (while keeping \mathbf{U} fixed) rescales the right hand sides of the differential equations (11) and (12) as well as the boundary conditions (17) by that same factor. These parameters thus satisfy the homogeneity assumption for F_ω in Eq. (9) and consequently the scaling invariance of steady states (Eq. 7). Further, one can readily identify several fluxes in the model, such as the gas exchange rate F_{CO_2} , the biological production rate J_{prod} , the DOP remineralization rate $\kappa_{\text{remin}}U_{\text{DOP}}$, the calcium carbonate export rate J_{Ca} , each of the source terms S_j , or the advective flux along any arbitrary direction ($\mathbf{u} \cdot \mathbf{v}U_j$, where the unit vector \mathbf{u} points in a specific direction of interest). Indeed, uniformly rescaling all focal parameters (while keeping \mathbf{U} fixed) will rescale each of these quantities by that same factor, thus satisfying the homogeneity assumption for fluxes in Eq. (13). Further, while these fluxes may be considered separately at any given location, one may instead also consider their averages, for example averaged over a specific geographic region or across the entire ocean. As an example, MCA may be used to determine the controls exerted by ocean currents, wind and waves (via κ_w), biological production (via α_{prod}) and remineralization (via κ_{remin}) on the overall CO_2 flux between the ocean and atmosphere.

S.2 Supplementary Discussion 2: Details of Black Sea SMTZ model

This section provides additional details on the structure, parameterization and simulation of the Black Sea SMTZ model discussed in the main text. Values of parameters mentioned are listed in Supplemental Table S1. Diffusivities of dissolved metabolites in the sediments, $D_j(z)$, were computed based on diffusivities in seawater, D_j^o , adjusted for sediment porosity at depth z , following the approach by Egger *et al.* [17]:

$$D_j(z) = \frac{D_j^o}{1 - 2 \ln(\phi(z))}, \quad (18)$$

where ϕ is the depth-dependent porosity:

$$\phi(z) = \phi_\infty + (\phi_0 - \phi_\infty) \cdot e^{-z/\gamma}, \quad (19)$$

and where ϕ_0 , ϕ_∞ and γ are parameters given in Supplemental Table S1. Seawater diffusivities D_j^o were computed using the marelac R package v2.1.11, for the in situ salinity and temperature. For the non-dissolved metabolites FeS and FeS₂, diffusivities were set to a small non-zero value for numerical stability. The down-

ward advection speed was set to:

$$v_j(z) = \frac{F_{\text{sed}}}{\rho \cdot (1 - \phi(z))} \quad (20)$$

for solids (FeS and FeS₂) and to

$$v_j(z) = \frac{F_{\text{sed}}}{\rho \cdot (1 - \phi_\infty)} \cdot \frac{\phi_\infty}{\phi(z)} \quad (21)$$

for dissolved metabolites (CH₄, Fe²⁺, H₂S and SO₄²⁻), where F_{sed} is the sedimentation rate and ρ is the sediment density at zero porosity [17, 18].

Simulation: To compute steady states, the PDE (Eq. 24 in main article) was simulated forward in time until convergence. Simulation was done using a centered finite difference scheme for partial derivatives, nested into a Runge-Kutta-Fehlberg (RK45) differential equation solver [19] implemented by the function `solve_ivp` in the python package `scipy v1.11.0` [20]. The spatial grid comprised 300 regularly spaced points. Initial concentrations at interior grid points were set to 0 for all metabolites. Simulation was done over multiple time periods, each lasting 1000 years and each starting from the last state of the previous period. Convergence to steady state was established if any one of the following conditions was met between successive periods: (A) The concentrations of all metabolites and at all grid points changed by less than 1 nM. (B) The relative change in concentration was less than 10^{-4} for each metabolite and at each grid point. (C) The normalized change in concentration was less than 10^{-4} for each metabolite and at each grid point, where the normalized change at any given grid point is defined as the change in value divided by the mean value across all grid points. For default parameter values, convergence was achieved after 10000 years based on criterion B.

Control coefficients: Partial derivatives needed for the control coefficients (Eqs. 10 and 15) were estimated via centered difference quotients, by varying focal parameters by 1% of their default value. For example, for a given flux J the FCC with respect to a given focal parameter p_i was estimated as:

$$\nu_i \approx \frac{p_i}{\bar{J}(\mathbf{p})} \cdot \frac{\bar{J}(\mathbf{p} + \varepsilon p_i \mathbf{e}_i) - \bar{J}(\mathbf{p} - \varepsilon p_i \mathbf{e}_i)}{2\varepsilon p_i}, \quad (22)$$

where $\mathbf{e}_i \in \mathbb{R}^m$ is the unit vector pointing along the i -th axis, $\varepsilon = 0.01$, and \bar{J} is the steady state flux computed for any given choice of parameters using the numerical scheme described earlier.

Table S1: Default parameter values used in the Black Sea SMTZ model. For additional derived parameters see Supplemental Text S.2.

symbol	description	value	reference
ϕ_0	porosity at surface	0.97	[17]
ϕ_∞	porosity at depth	0.61	[17]
ρ	sediment density	$2.31 \text{ g} \cdot \text{cm}^{-3}$	[17]
F_{sed}	sedimentation rate	$0.06 \text{ g} \cdot \text{cm}^{-2} \cdot \text{yr}^{-1}$	[17]
γ	porosity e-folding distance	95 cm	[17]
T	temperature	11°C	[17]
	pH	7.5	[21]
	salinity	22	[17]
$D_{\text{CH}_4}^o$	diffusivity of CH ₄ in seawater	$388.6 \text{ cm}^2 \cdot \text{yr}^{-1}$	marelac R package
$D_{\text{Fe}^{2+}}^o$	diffusivity of Fe ²⁺ in seawater	$150 \text{ cm}^2 \cdot \text{yr}^{-1}$	marelac R package
D_{FeS}^o	diffusivity of FeS in sediments	$1 \text{ cm}^2 \cdot \text{yr}^{-1}$	for numerical stability
$D_{\text{FeS}_2}^o$	diffusivity of FeS ₂ in sediments	$1 \text{ cm}^2 \cdot \text{yr}^{-1}$	for numerical stability
$D_{\text{H}_2\text{S}}^o$	diffusivity of H ₂ S in seawater	$377.6 \text{ cm}^2 \cdot \text{yr}^{-1}$	marelac R package
$D_{\text{SO}_4^{2-}}^o$	diffusivity of SO ₄ ²⁻ in seawater	$224.8 \text{ cm}^2 \cdot \text{yr}^{-1}$	marelac R package
β_{AOM}	affinity of AOM reaction	$63115 \text{ M}^{-1} \cdot \text{yr}^{-1}$	[22], Eq. (8)
β_{FIS}	affinity of FIS reaction	$1.5 \times 10^5 \text{ M}^{-1} \cdot \text{yr}^{-1}$	[17]
β_{FP}	affinity of FP reaction	$3250.4 \text{ M}^{-1} \cdot \text{yr}^{-1}$	[17]

Table S2: Boundary concentrations (mM) of metabolites in the Black Sea SMTZ model, based on measurements or model predictions by Egger *et al.* [17].

metabolite	top	bottom
CH ₄	0	13.5
Fe ²⁺	0	0.708
FeS	0	0
FeS ₂	0	0.02
H ₂ S	0	0
SO ₄ ²⁻	17.49	0

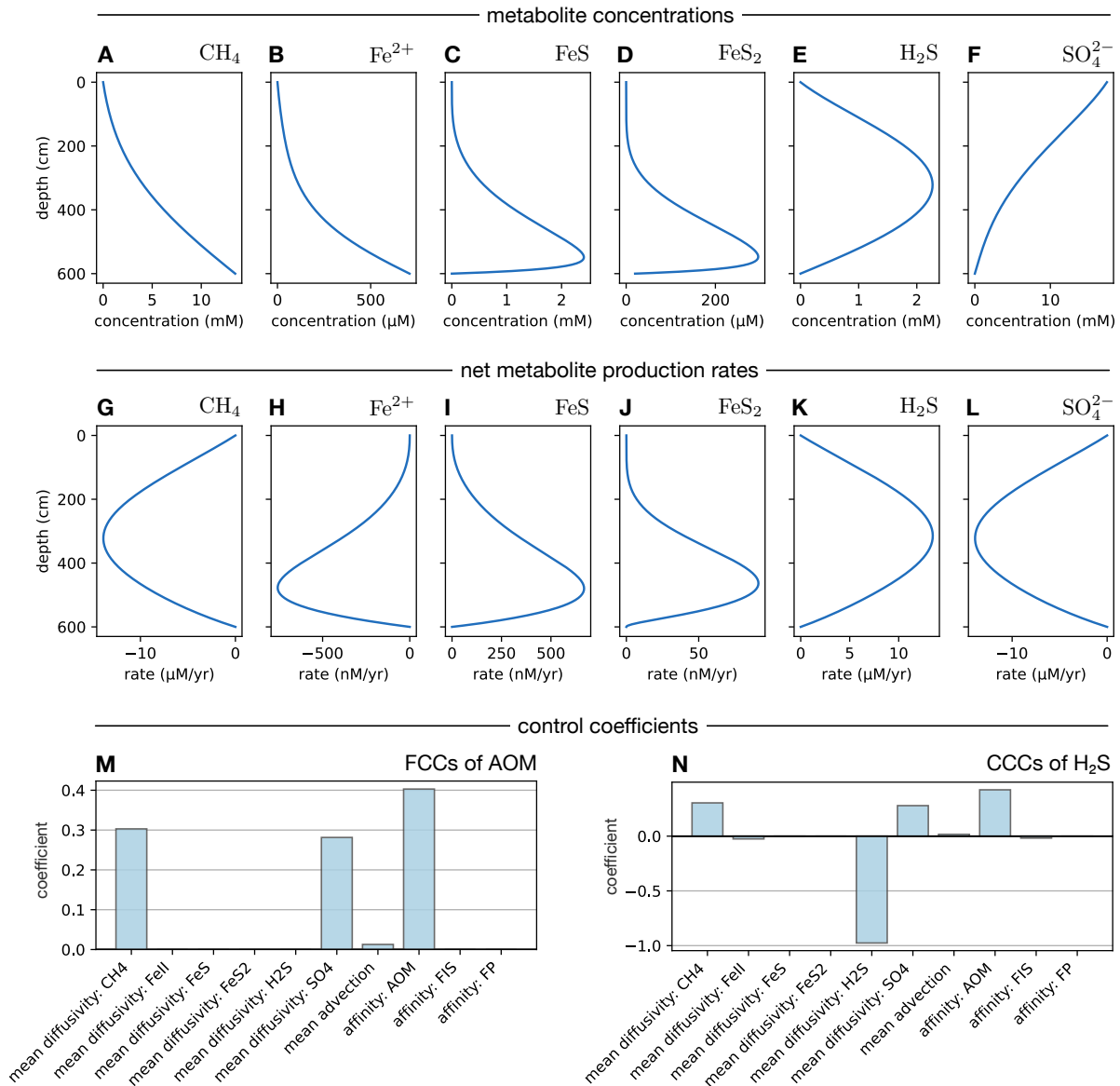


Figure S1: Black Sea SMTZ (slower reactions). (A–F) Steady state metabolite concentrations across the Black Sea sediment column (0–600 cm), as predicted by a modification of the PDE model where reaction affinities are 10^5 times lower. (G–L) Predicted steady state net production rates of metabolites. A negative rate indicates a net consumption. (M) Flux control coefficients for the rate of anaerobic methane oxidation (AOM). (N) Control coefficients for the average concentration of hydrogen sulfide.

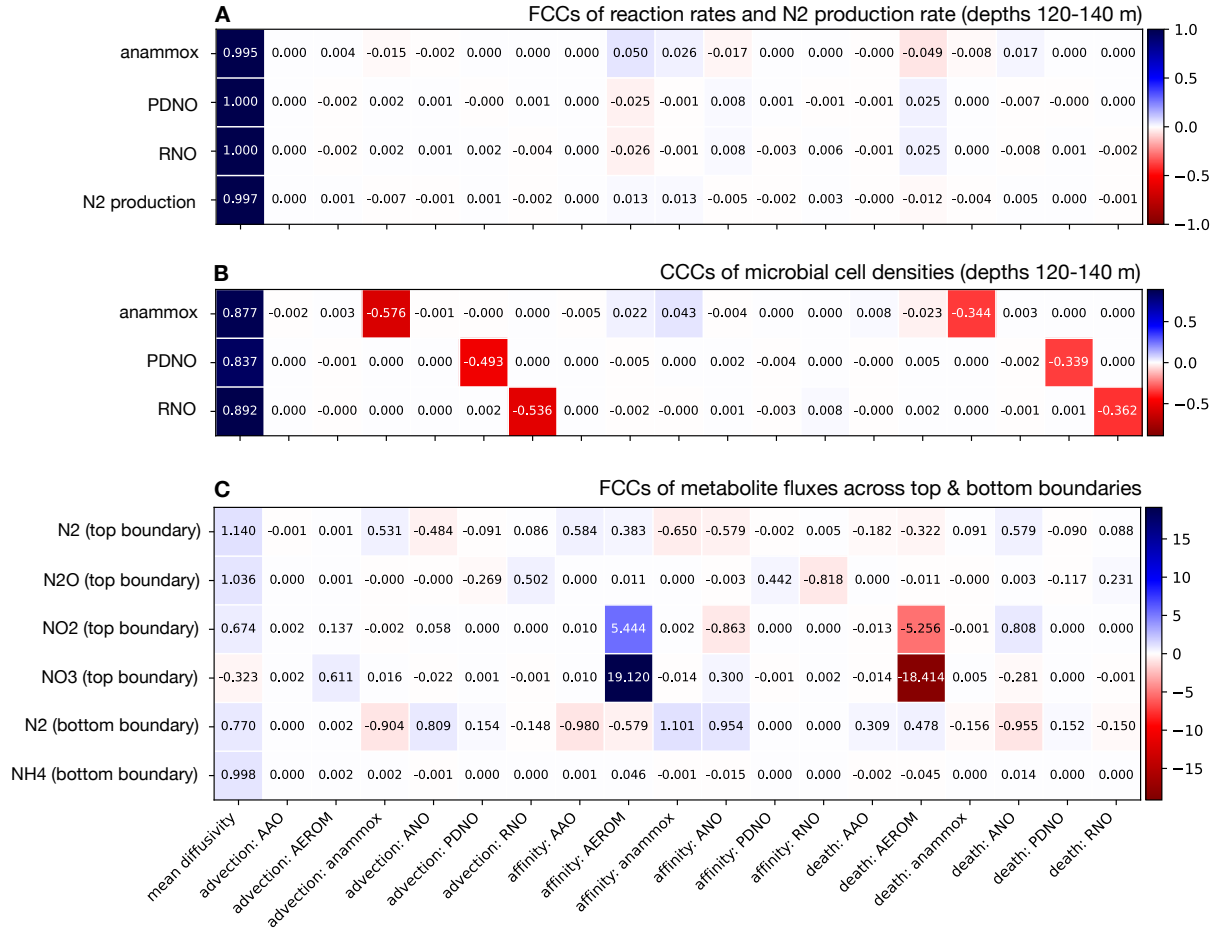


Figure S2: Saanich Inlet OMZ (redox interface and boundary fluxes). (A) FCCs for the mean rates of anammox, PDNO, RNO and total N₂ production within the depth interval 120–140 m. (B) CCCs of mean microbial densities associated with anammox, PDNO, RNO within the depth interval 120–140 m. (C) FCCs of flux rates across the top and bottom boundary, for various nitrogen compounds.

Supplementary References

- [1] Giersch, C. (1988) Control analysis of metabolic networks. *European Journal of Biochemistry* 174:509–513.
- [2] Acerenza, L., Sauro, H.M., and Kacser, H. (1989) Control analysis of time-dependent metabolic systems. *Journal of Theoretical Biology* 137:423–444.
- [3] Ap Rees, T. and Hill, S.A. (1994) Metabolic control analysis of plant metabolism. *Plant, Cell & Environment* 17:587–599.
- [4] Hofmeyr, J.H.S. (2001) Metabolic control analysis in a nutshell. In Proceedings of the 2nd International conference on systems biology, volume 2, pp. 291–300.
- [5] Moreno-Sánchez, R., Saavedra, E., Rodríguez-Enríquez, S., and Olín-Sandoval, V. (2008) Metabolic control analysis: A tool for designing strategies to manipulate metabolic pathways. *BioMed Research International* 2008:597913.
- [6] Cornish-Bowden, A. and Cárdenas, M.L. (2013) Control of metabolic processes, volume 190. Springer Science & Business Media.
- [7] Kacser, H., Burns, J.A., Kacser, H., and Fell, D. (1995) The control of flux. *Biochemical Society Transactions* 23:341–366.
- [8] Rosenzweig, M.L. and MacArthur, R.H. (1963) Graphical representation and stability conditions of predator-prey interactions. *American Naturalist* 97:209–223.
- [9] Pineda-Krch, M., Blok, J.H., Dieckmann, U., and Doebeli, M. (2007) A tale of two cycles—distinguishing quasi-cycles and limit cycles in finite predator–prey populations. *Oikos* 116:53–64.
- [10] Barraquand, F., Louca, S., Abbott, K.C., Cobbold, C.A., Cordoleani, F., DeAngelis, D.L., *et al.* (2017) Moving forward in circles: challenges and opportunities in modeling population cycles. *Ecology Letters* 20:1074–1092.
- [11] Dutkiewicz, S., Sokolov, A.P., Scott, J., and Stone, P.H. (2005) A three-dimensional ocean-seaice-carbon cycle model and its coupling to a two-dimensional atmospheric model: uses in climate change studies. Technical Report 122, MIT Joint Program of the Science and Policy of Global Change, Cambridge, MA, USA.
URL http://web.mit.edu/globalchange/www/MITJPSPGC_Rpt122.pdf
- [12] Marshall, J., Hill, C., Perelman, L., and Adcroft, A. (1997) Hydrostatic, quasi-hydrostatic, and nonhydrostatic ocean modeling. *Journal of Geophysical Research: Oceans* 102:5733–5752.
- [13] Marshall, J., Adcroft, A., Hill, C., Perelman, L., and Heisey, C. (1997) A finite-volume, incompressible Navier Stokes model for studies of the ocean on parallel computers. *Journal of Geophysical Research: Oceans* 102:5753–5766.
- [14] Sander, R. (2015) Compilation of Henry’s law constants (version 4.0) for water as solvent. *Atmospheric Chemistry and Physics* 15:4399–4981.
- [15] Wanninkhof, R. (1992) Relationship between wind speed and gas exchange over the ocean. *Journal of Geophysical Research: Oceans* 97:7373–7382.

- [16] Yamanaka, Y. and Tajika, E. (1996) The role of the vertical fluxes of particulate organic matter and calcite in the oceanic carbon cycle: Studies using an ocean biogeochemical general circulation model. *Global Biogeochemical Cycles* 10:361–382.
- [17] Egger, M., Kraal, P., Jilbert, T., Sulu-Gambari, F., Sapart, C.J., Röckmann, T., *et al.* (2016) Anaerobic oxidation of methane alters sediment records of sulfur, iron and phosphorus in the Black Sea. *Biogeochemistry* 13:5333–5355.
- [18] Meysman, F.J.R., Boudreau, B.P., and Middelburg, J.J. (2005) Modeling reactive transport in sediments subject to bioturbation and compaction. *Geochimica et Cosmochimica Acta* 69:3601–3617.
- [19] Fehlberg, E. (1970) Klassische Runge-Kutta-Formeln vierter und niedrigerer Ordnung mit Schrittweiten-Kontrolle und ihre Anwendung auf Wärmeleitungsprobleme. *Computing* 6:61–71.
- [20] Virtanen, P., Gommers, R., Oliphant, T.E., Haberland, M., Reddy, T., Cournapeau, D., *et al.* (2019) SciPy 1.0—Fundamental Algorithms for Scientific Computing in Python. *arXiv* arXiv:1907.10121.
- [21] Jørgensen, B.B., Böttcher, M.E., Lüschen, H., Neretin, L.N., and Volkov, I.I. (2004) Anaerobic methane oxidation and a deep H₂S sink generate isotopically heavy sulfides in Black Sea sediments. *Geochimica et Cosmochimica Acta* 68:2095–2118.
- [22] Devol, A.H., Anderson, J.J., Kuivila, K., and Murray, J.W. (1984) A model for coupled sulfate reduction and methane oxidation in the sediments of Saanich Inlet. *Geochimica et Cosmochimica Acta* 48:993–1004.